RESTRICTED

Copy No. 158

RM No. L9A07

NACA RM No. L9A07

NACA

RESEARCH MEMORANDUM

LOW-SPEED INVESTIGATION OF AILERON AND SPOILER CHARACTERISTICS OF A WING HAVING 42° SWEEPBACK OF THE LEADING EDGE AND CIRCULAR-ARC AIRFOIL SECTIONS AT REYNOLDS NUMBERS OF APPROXIMATELY 6.0×10^6

By

Stanley H. Spooner and Robert L. Woods

Langley Aeronautical Laboratory
Langley Air Force Base, Va.

NATIONAL ADVISORY COMMITTEE FOR AERONAUTICS

WASHINGTON

March 10, 1949

RESTRICTED

NATIONAL ADVISORY COMMITTEE FOR AERONAUTICS

RESEARCH MEMORANDUM

LOW-SPEED INVESTIGATION OF AILERON AND SPOILER CHARACTERISTICS OF A WING HAVING 42° SWEEPBACK OF THE LEADING EDGE AND CIRCULAR-ARC AIRFOIL SECTIONS AT REYNOLDS NUMBERS OF APPROXIMATELY 6.0×10^6

By Stanley H. Spooner and Robert L. Woods

SUMMARY

A low-speed investigation has been conducted in the Langley 19-foot pressure tunnel at Reynolds numbers from 5.3×10^6 to 6.9×10^6 to determine the effectiveness of a conventional aileron and of various spanwise spoiler arrangements on a 42° sweptback wing. The wing had an aspect ratio of 3.94, a taper ratio of 0.625, and thin, symmetrical, circular-arc airfoil sections. The rolling-moment characteristics of the aileron and the spoilers, together with the aileron hinge-moment, normal-force, and balance-chamber pressure characteristics were determined for both the plain wing and the wing equipped with various high-lift and stall-control devices.

The results of the investigation indicate that the effectiveness of the aileron C_{l_δ} on the plain wing decreased slightly at high angles of attack. At low angles of attack, the effectiveness of the aileron was approximately the same regardless of the flap configuration. As the angle of attack was increased, however, deflection of inboard-located, half-span, split flaps resulted in a loss of aileron effectiveness. The combination of leading-edge flaps and stall-control fences almost entirely offset the detrimental effects which resulted when the split flaps were deflected. For the plain wing configuration, the aileron hinge-moment characteristics were such that a conventional, sealed, internal aerodynamic balance of approximately 30 percent of the aileron chord would be required to completely balance the aileron at low angles of attack. With this amount of balance, the aileron probably would be underbalanced at high angles of attack of the plain wing and at all angles of attack of the flapped configurations. When stalling occurred on the outboard portions of the wing, as it did without the stall-control devices, an inboard spoiler location was more effective than an outboard location, and when inboard stalling occurred the outboard spoiler location proved more effective. The spoilers on the plain wing became ineffective in the maximum lift range. The maximum rolling effectiveness of the 10-percent-chord step spoilers on the wing equipped with the high-lift and stall-control devices was equivalent to that produced by a total aileron deflection of approximately 35°.

INTRODUCTION

The contemplated use of swept wings incorporating sharp-edged airfoil sections for high-speed airplanes has resulted in a need for information concerning the effectiveness of lateral-control devices on wings of this type. An investigation at low air speeds, therefore, has been made in the Langley 19-foot pressure tunnel to determine the lateral characteristics of a 42° sweptback wing which had sharp-edged, symmetrical, circular-arc airfoil sections and was equipped with either a conventional aileron or various spanwise arrangements of step spoilers.

The rolling-moment characteristics of the aileron and the spoilers together with the aileron hinge-moment, normal-force, and balance-chamber pressure characteristics were determined for both the plain wing and the wing equipped with various high-lift and stall-control devices. These devices included extensible, round-nose, leading-edge flaps, leading-edge drooped-nose flaps, trailing-edge split flaps, and upper-surface fences.

The investigation was conducted at Reynolds numbers ranging between 5.3×10^6 and 6.9×10^6 which corresponded to a Mach number range of 0.11 to 0.15.

SYMBOLS

The data are referred to a set of axes coinciding with the wind axes and originating in the plane of symmetry at the quarter-chord point of the mean aerodynamic chord. All wing coefficients are based upon the dimensions of the basic wing.

C_L lift coefficient (Lift/qS)

$C_{L_{max}}$ maximum lift coefficient

C_D drag coefficient (Drag/qS)

C_m pitching-moment coefficient (Pitching moment/qS$\bar{c}$)

C_n yawing-moment coefficient (Yawing moment/qSb)

C_l rolling-moment coefficient (Rolling moment/qSb)

C_{N_a} aileron normal-force coefficient (Aileron normal force/qS_a)

C_{h_a} aileron hinge-moment coefficient $\left(\text{Aileron hinge moment about hinge line}/qb_a\bar{c}_a^{\,2}\right)$

P_R aileron balance-chamber resultant-pressure coefficient ((Lower-surface pressure - Upper-surface pressure)/q)

q free-stream dynamic pressure, pounds/square foot

b wing span measured normal to plane of symmetry, feet

b_s spoiler span measured normal to plane of symmetry, feet

$b_a\bar{c}_a^{\,2}$ product of aileron span, measured along aileron hinge line, and square of root-mean-square chord, measured behind and normal to hinge line, 0.536 cubic feet

S wing area, square feet

S_a aileron area behind hinge line, square feet

$\bar{c}$ wing mean aerodynamic chord measured parallel to plane of symmetry, 2.942 feet $\left(\frac{2}{S}\int_0^{b/2} c^2 dy\right)$

c local wing chord measured parallel to plane of symmetry, feet

$\bar{c}_b$ root-mean-square chord of hypothetical aileron balance measured ahead of and normal to aileron hinge line, feet

y spanwise coordinate, measured normal to plane of symmetry, feet

α angle of attack, degrees

δ_a aileron deflection, measured in plane normal to hinge line, degrees (positive when trailing edge is deflected downward)

$\delta_{a_{total}}$ arithmetical sum of equal up and down aileron deflections for an assumed set of ailerons

Λ sweepback of leading edge of wing, degrees

C_{l_δ} rate of change of rolling-moment coefficient with aileron deflection (aileron effectiveness)

C_{h_δ} rate of change of hinge-moment coefficient with aileron deflection

C_{h_α} rate of change of hinge-moment coefficient with angle of attack

P_{R_δ} rate of change of aileron-balance-chamber pressure coefficient with aileron deflection

P_{R_α} rate of change of aileron-balance-chamber pressure coefficient with angle of attack

C'_{h_δ} rate of change of hinge-moment coefficient in a steady roll with aileron deflection

MODEL

The principal dimensions of the model are shown in figure 1. Photographs of the model mounted in the Langley 19-foot pressure tunnel are shown in figure 2. The wing was of solid steel construction and had an aspect ratio of 3.94 and a taper ratio of 0.625. A straight line connecting the leading edge of the root and theoretical tip chords was swept back 42.05°. The symmetrical circular-arc airfoil sections were fabricated with a constant radius of 83.26 inches in a plane perpendicular to the line of maximum thickness. As a result, the leading and trailing edges were slightly curved in plan form. The maximum divergence from a straight line connecting the root and theoretical tip chords at the leading and trailing edges was about 0.4 inch. The airfoil sections, taken normal to the line of maximum thickness, had a maximum thickness of 10 percent of the chord at the root and 6.4 percent of the chord at the tip. Parallel to the plane of symmetry the maximum thickness was 7.9 percent of the chord at the root and 5.2 percent of the chord at the tip.

The high-lift and stall-control devices used on the model are shown in figure 3. The drooped-nose flaps extended over the outer 60 percent of the wing, had a chord of 0.184c, and were deflected 30° measured in a plane normal to the hinge line. The amount of flap deflection was based upon unpublished data which indicated 30° to be optimum for this wing from considerations of pitching moment and maximum lift. The extensible leading-edge flaps had a span of $0.55\frac{b}{2}$ and extended from $0.425\frac{b}{2}$ to $0.975\frac{b}{2}$ (beginning of rounded tip). The chord was constant and amounted

to about 18 and 13 percent of the wing chord at the outboard and inboard ends, respectively. The deflection was 37°, measured in the manner shown in figure 3. The 0.20c trailing-edge split flaps extended over the inboard 50 percent of the wing semispan and were deflected 60° from the lower surface of the wing.

The upper-surface fences (fig. 3) were mounted normal to the wing surface and parallel to the plane of symmetry. They projected 0.6 of the maximum thickness of the root section above the wing surface. When used in conjunction with the drooped-nose flaps, the fences extended from the wing trailing edge to about the 0.18c point and were located $0.05\frac{b}{2}$ outboard of the inboard ends of the drooped-nose flaps. For the configurations with the extensible leading-edge flaps, the fences extended from the trailing edge to the leading edge of the wing and were located $0.025\frac{b}{2}$ outboard of the inboard ends of the flaps.

Only the left side of the wing was equipped with the sealed, unbalanced, contour aileron. The aileron chord was about 0.18c, and the span was $0.475\frac{b}{2}$, with the inboard end located at $0.5\frac{b}{2}$. Resistance-type electrical strain gages were employed to measure the aileron normal forces and hinge moments. The aileron seal, which was designed in a manner so that no moments and negligible forces were transferred from it to the aileron, extended the full span of the aileron except for cut-outs to allow for the mounting of the strain-gage beams. Pressure orifices were installed in the aileron balance chamber to enable the pressure differences across the seal to be determined. The details of the aileron are given in figure 4.

The spoilers used were of the step type. The span of each step was $0.10\frac{b}{2}$ with the exception of the outboard one which was $0.075\frac{b}{2}$. With all steps in place, the spoilers extended from the $0.20\frac{b}{2}$ station outboard to the $0.975\frac{b}{2}$ station. Spoiler projections of 0.05c and 0.10c were tested. The spoilers were normal to the wing surface and to the plane of symmetry. They were located on the 0.70c line of the left wing panel in the manner shown in figure 4.

TESTS

The tests were made in the Langley 19-foot pressure tunnel with the air in the tunnel compressed to approximately $2\frac{1}{3}$ atmospheres. Measurements of the lift and drag and the pitching, rolling, and yawing moments

were made for each configuration through an angle-of-attack range extending from -4° to beyond maximum lift. For the aileron tests the normal forces, hinge moments, and balance-chamber pressures of the aileron were determined for aileron deflections ranging from 25° to -25°. The spoiler tests were made by using various spans of step spoilers, in increments of approximately 20 percent of the semispan, starting either from $0.975\frac{b}{2}$ or $0.20\frac{b}{2}$ spanwise stations. The stall studies were made by visual observation and from motion-picture records of the behavior of wool tufts attached to the upper surface of the wing.

All of the spoiler tests and the stall studies were conducted at a Mach number of 0.15 and a Reynolds number of 6.9×10^6, based on the wing mean aerodynamic chord. The aileron tests, with the exception of the plain wing configuration which was tested at a Reynolds number of 6.9×10^6, were conducted at a Reynolds number of 5.3×10^6 and a Mach number of 0.11. Scale-effect tests were not made, since reference 1 has indicated no appreciable scale effect in this Reynolds number range.

REDUCTION OF DATA

All data have been reduced to standard nondimensional coefficients. Corrections have been applied to the force and moment data to account for the tare and interference effects of the model support system. Stream-inclination and jet-boundary corrections have been applied to the angle of attack and to the drag and pitching-moment coefficients. Jet-boundary corrections to the rolling- and yawing-moment coefficients were found to be negligible and, therefore, were not applied to the data.

The aileron hinge-moment coefficients presented herein are based upon the product of the aileron span and the square of the root-mean-square chord. Some recent practice (reference 2) has based the hinge-moment coefficients upon twice the area moment of the aileron. The coefficients presented herein may be converted to this base by means of the following equation:

$$C_{h_a} \text{ (based on twice area moment)} = 0.952C_{h_a} \text{ (presented herein)} \quad (1)$$

As a result of the interference of the strain-gage beams, the aileron seal was incomplete and a small amount of leakage across it occurred. A calibration of the leakage was made, and the resultant pressure coefficients corrected to a no-leakage condition. The effect of the leakage on the rolling-moment and hinge-moment coefficients is believed to be small and has been neglected.

RESULTS AND DISCUSSION

Aileron Characteristics

Rolling characteristics.- The basic aileron data are shown in figures 5 to 10. Several representative crossplots of C_l and C_{h_a} against aileron deflection are presented in figures 11 and 12, respectively. In order to show the aileron effectiveness C_{l_δ} determined for a small range of aileron deflections through $\delta_a = 0^\circ$, the variation of C_{l_δ} with angle of attack is presented in figure 13 for the several flap arrangements tested.

It can be seen that C_{l_δ} has a value of approximately 0.00100 at low angles of attack for all flap configurations. The value of C_{l_δ} of 0.00105 obtained at $\alpha = 0^\circ$ for the wing without flaps was about the same as that (0.00102) determined by means of the charts of reference 3 and reduced by $\cos^2\Lambda$ to account for the effects of sweep. The rate of change of rolling-moment coefficient with aileron deflection C_{l_δ} for the wing without flaps and for the wing equipped with the extensible leading-edge flaps and fences remained approximately constant as the angle of attack was increased up to that corresponding to $0.85C_{L_{max}}$. The lift coefficients corresponding to $0.85C_{L_{max}}$ are used herein as a basis for comparison since they might be considered as representative of those for the landing-approach condition. The addition of the split flaps to the plain wing resulted in a 25-percent decrease in C_{l_δ} at $0.85C_{L_{max}}$. Furthermore at $C_{L_{max}}$, the value of C_{l_δ} was only 0.00040. The further addition of the leading-edge flaps did not prevent the large reduction caused by the split flaps but, with the leading-edge flaps in combination with the stall-control fences, the values of C_{l_δ} were comparable to those obtained for the plain wing. The aileron effectiveness of the wing equipped with the drooped-nose and split flaps and fences was approximately the same as that for the configuration with the extensible leading-edge and split flaps and fences.

From an inspection of the basic data presented in figures 5 to 10, it can be seen that the rolling-moment coefficients obtained from the plain wing and the split-flap configurations were approximately the same for either up or down aileron deflections. For the configurations having the leading-edge devices, however, the rolling-moment coefficients produced by the ailerons were larger for the up deflections than for the down deflections.

The rolling-moment coefficients obtained for a total aileron deflection of 30° (15° up and 15° down) on the various wing configurations are presented in figure 14. The rolling-moment coefficients produced by large deflections of the ailerons varied considerably with wing configuration and with angle of attack. At these large aileron deflections the total rolling-moment coefficients at low angles of attack were approximately the same (about 0.03) for all configurations investigated. At higher angles of attack the total rolling-moment coefficients produced by large deflections of the aileron on the different configurations varied in a manner similar to the aileron effectiveness at small deflections in that the rolling-moment coefficients obtained with the split flap configuration decreased rapidly with increasing angle of attack. Only moderate decreases were obtained with the configurations involving the leading-edge and split flaps and the fences. With the leading-edge flaps and fences but without the split flaps the decrease was slight.

Adverse yawing-moment coefficients were obtained throughout most of the angle-of-attack range, the largest values of which were obtained for the wing without flaps (fig. 14).

Pitching-moment characteristics.- The curves of pitching-moment coefficient against angle of attack for the maximum aileron deflections investigated are presented in figures 5 to 10. It can be seen that for the plain wing and for the wing equipped with split flaps a smaller increment in the pitching-moment coefficient was obtained at positive angles of attack with the up aileron than with the down aileron. Conversely, smaller increments in the pitching-moment coefficient were obtained with the down aileron than with the up aileron for the wing equipped with the leading-edge devices. It is estimated that about 2° of elevator deflection would be needed to compensate for the maximum increment in pitching-moment coefficient resulting from 25° up and down deflection of a set of ailerons.

Hinge-moment characteristics.- In order to illustrate the aileron hinge-moment characteristics of the various configurations investigated, the hinge-moment parameters C_{h_δ} and C_{h_α} and the balance-chamber resultant-pressure parameters P_{R_δ} and P_{R_α} were determined from the

basic data of figures 5 to 10 and are presented in figure 15. It can be seen that considerable variation in the values of these parameters occurred. In order to show the effects of the variation in C_{h_α}, a rolling condition must be considered, and if the aileron balance is to be of the conventional, sealed, internally balanced type, the parameters P_{R_δ} and P_{R_α} also must be considered. The combined effect of these parameters for an aileron having various amounts of internal balance is shown in figure 16. The hinge-moment parameters of the aileron with varying amounts of balance were calculated by means of the following equations:

$$C_{h_\delta \text{ with balance}} = C_{h_\delta \text{ without balance}} + \frac{1}{2} P_{R_\delta} \left(\frac{\bar{c}_b}{\bar{c}_a} \right)^2 \tag{2}$$

$$C_{h_\alpha \text{ with balance}} = C_{h_\alpha \text{ without balance}} + \frac{1}{2} P_{R_\alpha} \left(\frac{\bar{c}_b}{\bar{c}_a} \right)^2 \tag{3}$$

where the span of the balance was assumed equal to the span of the aileron and where the balance chord was assumed to include one-half of the gap covered by the seal.

The parameter C'_{h_δ} is defined as the rate of change of hinge-moment coefficient in a steady roll with aileron deflection and was calculated by means of the following equation:

$$C'_{h_\delta} = C_{h_\delta} + \frac{2(\Delta\alpha)_p}{\Delta\delta_a} C_{h_\alpha}$$

in which the values of the parameters C_{h_δ} and C_{h_α} were computed from equations (2) and (3) for various amounts of balance and where $\frac{2(\Delta\alpha)_p}{\Delta\delta_a} = K \frac{C_{l_\delta}}{C_{l_p}} = -210 C_{l_\delta}$ and is the ratio of the effective change in angle of attack in a steady roll to the change in aileron deflection. The constant K was determined by means of the charts of reference 4. The damping-in-roll coefficient C_{l_p} was determined from reference 5 and had a value of 0.266.

Considering first the aileron without any internal balance, figure 16 shows that on the plain wing the aileron was more underbalanced at high angles of attack than it was at low angles of attack. The addition of the split flaps resulted in an opposite effect; the aileron was more balanced at high than at low angles of attack. The further addition of the leading-edge flaps and the stall-control fences tended to offset the effect of the split flaps and resulted in a reduction in the variation of C'_{h_δ} through the angle-of-attack range. The values of C'_{h_δ} at high angles of attack and for the flapped configurations are not necessarily correct since C_{l_p}, which was determined at $\alpha = 0^\circ$ for the plain wing and assumed constant in the determination of C'_{h_δ}, probably varies with angle of attack and flap configuration. The trends, however, are considered to be indicative of the effects of the high-lift and stall-control devices.

The data presented in figure 16 indicate that on the plain wing at zero angle of attack this aileron equipped with a conventional, sealed internal balance would require a balance chord of about 30 percent of the aileron chord for $C'_{h_\delta} = 0$. As the angle of attack is increased, more balance chord is required until at about the angle of attack for $C_{L_{max}}$ a balance chord of approximately 55 percent would be required. For the split-flap configuration the amount of balance chord required for $C'_{h_\delta} = 0$ was 45 percent at $\alpha = 0^\circ$, increased to more than 55 percent at moderate angles of attack, and then decreased to about 45 percent at high angles of attack. For the configurations involving the leading-edge devices and the fences, the amount of balance chord required for $C'_{h_\delta} = 0$ was between 45 and 50 percent at low angles of attack and increased about 5 percent at the angles of attack corresponding to $0.85C_{L_{max}}$.

If, therefore, the aileron on the plain wing was closely balanced for the high-speed condition, it would be underbalanced at the low-speed, flaps-deflected condition although the small dynamic pressures at the low speeds would tend to prevent the occurrence of excessive control forces.

The foregoing comparison of the aileron effectiveness for the various flap configurations has been made by using slopes determined at zero aileron deflection. Since the data presented in figure 12 indicate

that the variation of hinge-moment coefficient with aileron deflection becomes more negative at large deflections, it should be noted that the aileron would be more underbalanced at these large deflections than is indicated in figure 16.

Normal-force characteristics.- The aileron normal-force coefficients presented in figures 5 to 10 represent the forces on the aileron behind the hinge line. In the use of these data in the design of an aileron with a sealed internal balance, account must be taken of the additional forces acting on the balance. The maximum values of the aileron normal-force coefficients were about the same for the flapped or unflapped wing configurations. The stall studies presented in figure 17 show that the aileron on the plain wing is completely stalled at an angle of attack of 16.9°, whereas the aileron on the flapped wing is only partly stalled at angles of attack of more than 19°. As a result of this early aileron stall the variation of aileron normal-force coefficient with angle of attack for the plain wing was not as linear as that for the wing with the leading-edge devices.

Spoiler Characteristics

Representative data obtained from tests of numerous wing and spoiler configurations are presented in figures 18 to 21.

Rolling-moment characteristics.- It is apparent from the data presented in figures 18 to 21 that the origin and progression of the stall are reflected in the rolling-moment coefficients contributed by the various spoiler arrangements. In the case of the plain wing (fig. 18(a)), the outboard section of the $0.775\frac{b}{2}$ spoiler is enveloped in tip stall at a relatively low angle of attack (approximately 8.6°; fig. 17) which results in an abrupt decrease in C_l. The same abrupt decrease in C_l is indicated for a $0.375\frac{b}{2}$ spoiler located at the tip, whereas a $0.4\frac{b}{2}$ spoiler located inboard of the $0.60\frac{b}{2}$ station does not encounter the effects of the wing stall until an angle of attack of approximately 12°. The wing equipped with the high-lift and stall-control devices exhibited an initial stalled region behind the inboard ends of the leading-edge flaps, and as the spoilers extended into this region there was a marked reduction in C_l (figs. 20 and 21(a)). It should be noted that for the flapped configurations some rolling-moment coefficient is produced for angles of attack corresponding to $C_{L_{max}}$.

The effects of spoiler projection or height for the plain wing may be seen by a comparison of figures 18(a) and 19(a). In the low angle-of-attack range, the 0.10c spoiler is several times as effective as the 0.05c spoiler which in all probability is due to the fact that a smaller percentage of the 0.10c spoiler is in the boundary-layer air. At the angles of attack where the boundary layer becomes thicker and flow separation occurs, the effectiveness of both the 0.10c and 0.05c spoilers becomes equal until finally both have zero effectiveness as all the spoiler segments are enveloped in the stalled region.

In figures 22 to 24 a summary is presented of all spoiler combinations tested. It can be seen in figure 22 that for a given spoiler span on the plain wing the inboard location provided slightly greater values of C_l at low angles of attack than did the outboard location. It is quite possible that the inboard spoilers on a sweptback wing can, due to crossflow, cause spoiling of the flow over sections of the wing outboard of the spoilers. For the flaps-deflected configurations, a spoiler located on the outboard portion of the wing produced higher values of C_l than a spoiler of equal span located inboard. A spoiler of the same span but with its inboard end located at the wing root might result in yet different results. It seems, therefore, that the optimum spanwise spoiler location on a sweptback wing is largely dependent upon the span loading and/or the spanwise center of pressure of that particular wing.

It can be seen in figure 22 that for the plain wing equipped with a short span of the 0.05c spoilers some rolling-moment reversal was encountered. It is possible that with a short span of the 0.10c spoilers reversal might also be encountered. For this reason no attempt has been made to fair the curves of figures 22 to 24 through $\frac{b_s}{b/2} = 0$.

Other aerodynamic characteristics.- As indicated in figures 18 to 21, the yawing-moment coefficients obtained with the spoilers on the plain wing were favorable up to an angle of attack of about 12°. Above this angle, adverse yawing-moment coefficients were obtained although the values were small. The addition of leading-edge and trailing-edge flaps resulted in favorable yawing-moment characteristics up to almost the angle of attack for $C_{L_{max}}$. The values of C_n at the lower angles of attack were somewhat larger for the wing with flaps than for the plain wing.

The maximum changes in the pitching-moment coefficient resulting from the 0.10c projection of the spoilers were 50 to 100 percent greater than those resulting from the maximum deflection of a set of ailerons. The outboard spoilers on the plain wing configuration caused a large positive shift in the pitching-moment curve up to the angle of attack at which tip stalling began. As the separated flow at higher angles of

attack encompassed the spoilers, the spoiler effectiveness dropped off and the pitching-moment coefficients became approximately the same as for the wing without spoilers (fig. 18). A large positive shift in the pitching-moment curves, which occurred throughout the angle-of-attack range, was obtained with the outboard spoilers on the flapped configurations as shown in figure 21. This trim change probably occurred as a result of the outboard spoiler segments remaining in regions of unseparated flow at all angles of attack. In all cases where trim changes occurred, larger changes were encountered with the outboard spoiler locations than with the inboard locations. The magnitude of the trim change was also dependent upon the spoiler projection.

Comparison of Aileron and Spoilers

A brief comparison of the relative rolling effectiveness of the aileron and the spoilers is presented in figure 25. The comparison is made using what is considered as the optimum spoiler span and location as determined from data presented in figures 22 and 23; namely, $0.60\frac{b}{2}$, the inboard end being located at $0.20\frac{b}{2}$ and $0.375\frac{b}{2}$ spanwise stations for the plain wing and the flapped configurations, respectively. It can be seen that for the plain wing the rolling-moment coefficient at small angles of attack produced by the 0.10c projection spoilers was approximately equal to that which would be produced by a total aileron deflection of 25°. At higher angles of attack, however, the rolling effectiveness of the spoilers dropped to zero, whereas the aileron maintained considerable effectiveness up through the highest angle of attack investigated. For the wing equipped with the extensible leading-edge flaps and the split flaps, the spoilers produced rolling-moment coefficients through the high angle-of-attack range which were equivalent to about 35° of total aileron deflection. Although the rolling effectiveness of the aileron increased about linearly with deflection up to $\delta_a = \pm 25°$, the use of large deflections for ailerons equipped with conventional internal-balance systems is limited on thin wings of the type investigated herein to about ±15° for a 30-percent balance chord.

The value of the wing-tip helix angle produced in a steady roll by a lateral-control device is indicative of the power or effectiveness of that device. The helix angles were therefore estimated as C_l/C_{l_p} where C_{l_p} is the damping-in-roll coefficient. With the aileron deflection limited to about ±15° the value of the helix angle obtainable at $0.85C_{L_{max}}$ with the flaps-deflected configuration would be about 0.084 for the aileron and 0.093 for the 0.10c projection spoilers. This difference between the values of the helix angle produced by the aileron and by the spoiler would probably be even greater if account were taken of the adverse yawing-moment characteristics at the lower speeds.

The foregoing comparison was based on the assumption that the stick force of the aileron control would be held within range of pilot capabilities through the use of an internal aerodynamic balance and that the aileron deflection would be limited to $\pm 15^{\circ}$ by this balance. Under such conditions the maximum effectiveness of the spoilers can be expected to be as good as or superior to that of the aileron except for the plain wing at high angles of attack. If, however, by employment of some means of power boost aileron deflections up to $\pm 25^{\circ}$ could be obtained, the aileron rolling effectiveness would be considerably superior to that of the spoiler.

CONCLUSIONS

The results of an investigation in the Langley 19-foot pressure tunnel of the characteristics of two types of lateral-control devices on a 42° sweptback wing with circular-arc airfoil sections and various high-lift and stall-control devices indicated the following conclusions:

1. The effectiveness of the aileron C_{l_δ} on the plain wing decreased slightly at high angles of attack. At low angles of attack the effectiveness of the aileron was approximately the same regardless of the flap configuration. As the angle of attack was increased, however, deflection of inboard-located half-span split flaps resulted in a considerable loss of aileron effectiveness. The combination of leading-edge flaps and stall-control fences tended to offset the detrimental effects which resulted when the split flaps were deflected.

2. The aileron hinge-moment characteristics were such that a conventional, sealed, internal aerodynamic balance of approximately 30 percent of the aileron chord would be required to completely balance the aileron at low angles of attack of the plain wing configuration. With this amount of balance the aileron probably would be underbalanced at high angles of attack of the plain wing and at all angles of attack of the flapped configurations.

3. The rolling effectiveness of the spoiler at high angles of attack appears largely dependent upon the spoiler location with respect to the areas of separated flow on the wing. When stalling occurred on the outboard portions of the wing an inboard spoiler location was more effective. When stalling occurred inboard, as it did with the wing equipped with the stall-control devices, the outboard spoiler location was more effective.

4. The spoilers on the plain wing became ineffective in the maximum lift range. The maximum rolling effectiveness of the 0.10c spoilers on the wing equipped with the high-lift and stall-control devices was equivalent to that produced by a total aileron deflection of approximately 35°.

Langley Aeronautical Laboratory
National Advisory Committee for Aeronautics
Langley Air Force Base, Va.

REFERENCES

1. Neely, Robert H., and Koven, William: Low-Speed Characteristics in Pitch of a 42° Sweptback Wing with Aspect Ratio 3.9 and Circular-Arc Airfoil Sections. NACA RM No. L7E23, 1947.

2. Fischel, Jack, and Schneiter, Leslie E.: An Investigation at Low Speed of a 51.3° Sweptback Semispan Wing Equipped with 16.7-Percent-Chord Plain Flaps and Ailerons Having Various Spans and Three Trailing-Edge Angles. NACA RM No. L8H20, 1948.

3. Weick, Fred E., and Jones, Robert T.: Résumé and Analysis of N.A.C.A. Lateral Control Research. NACA Rep. No. 605, 1937.

4. Langley Research Department (Compiled by Thomas A. Toll): Summary of Lateral-Control Research. NACA Rep. No. 868, 1947.

5. Toll, Thomas A., and Queijo, M. J.: Approximate Relations and Charts for Low-Speed Stability Derivatives of Swept Wings. NACA TN No. 1581, 1948.

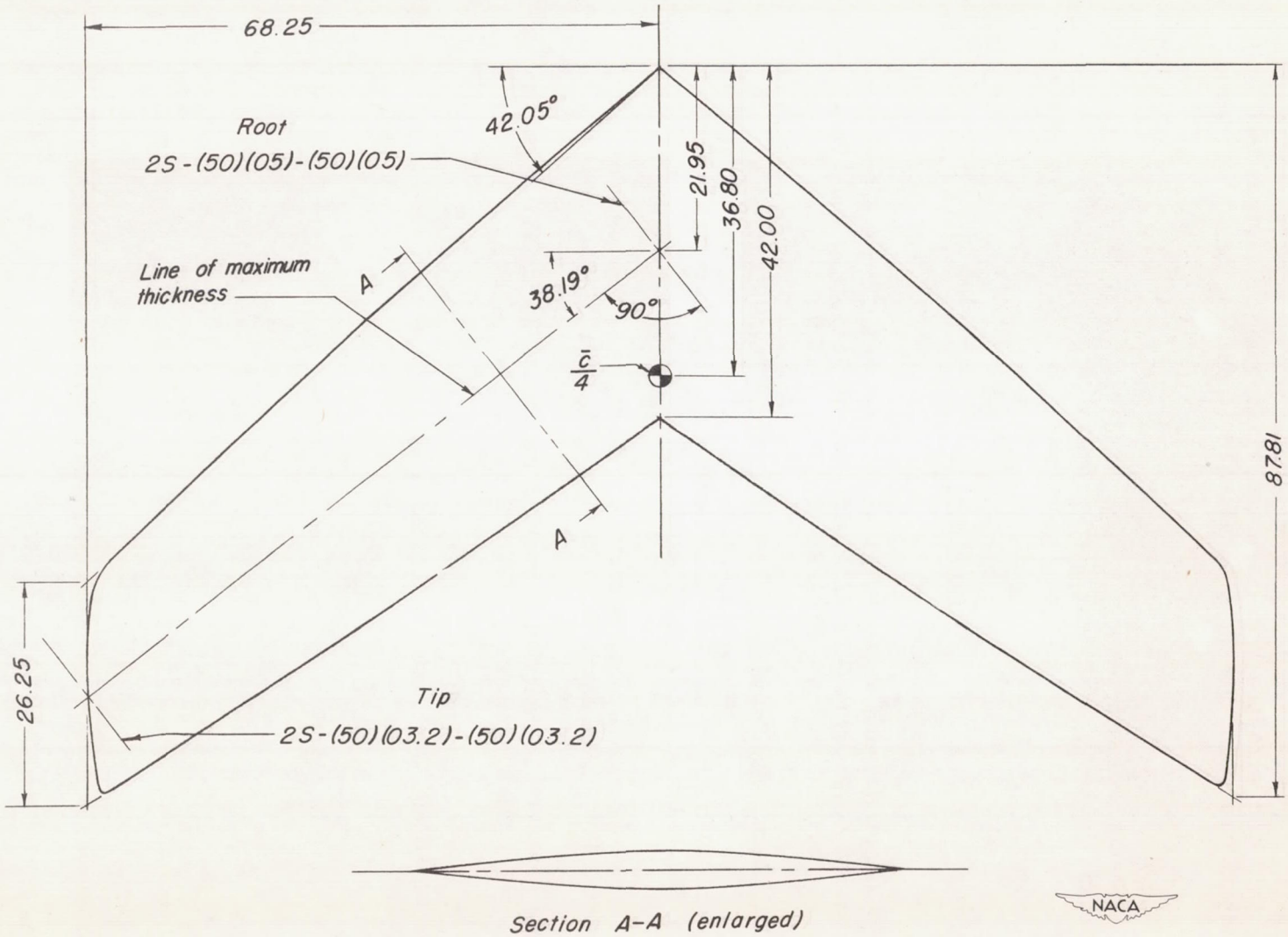

Figure 1.- Geometry of wing. All dimensions in inches.

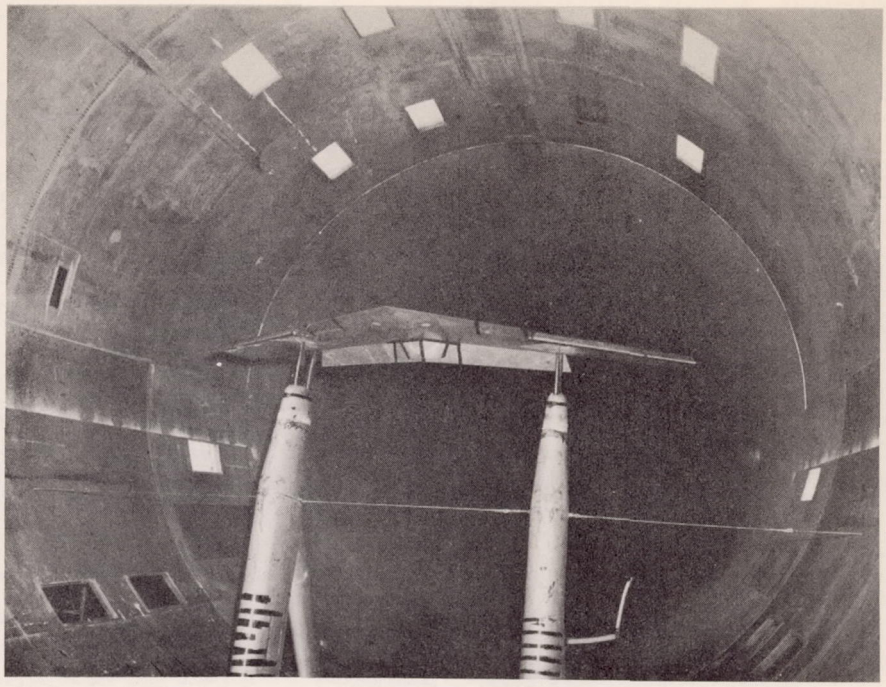

(a) Front view of bottom of wing.

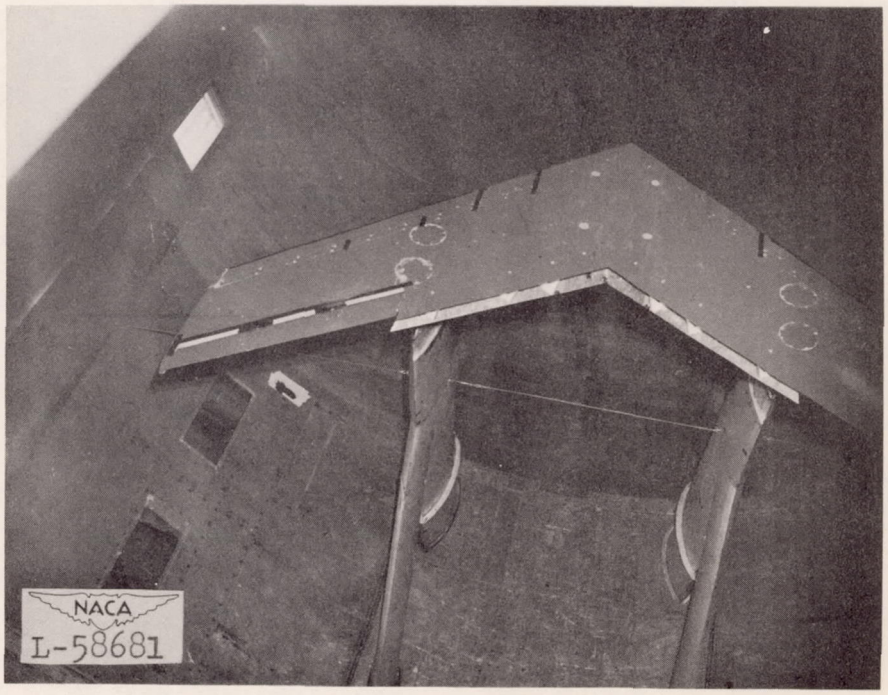

(b) Rear view of top of wing.

Figure 2.– Wing mounted in 19–foot pressure tunnel.

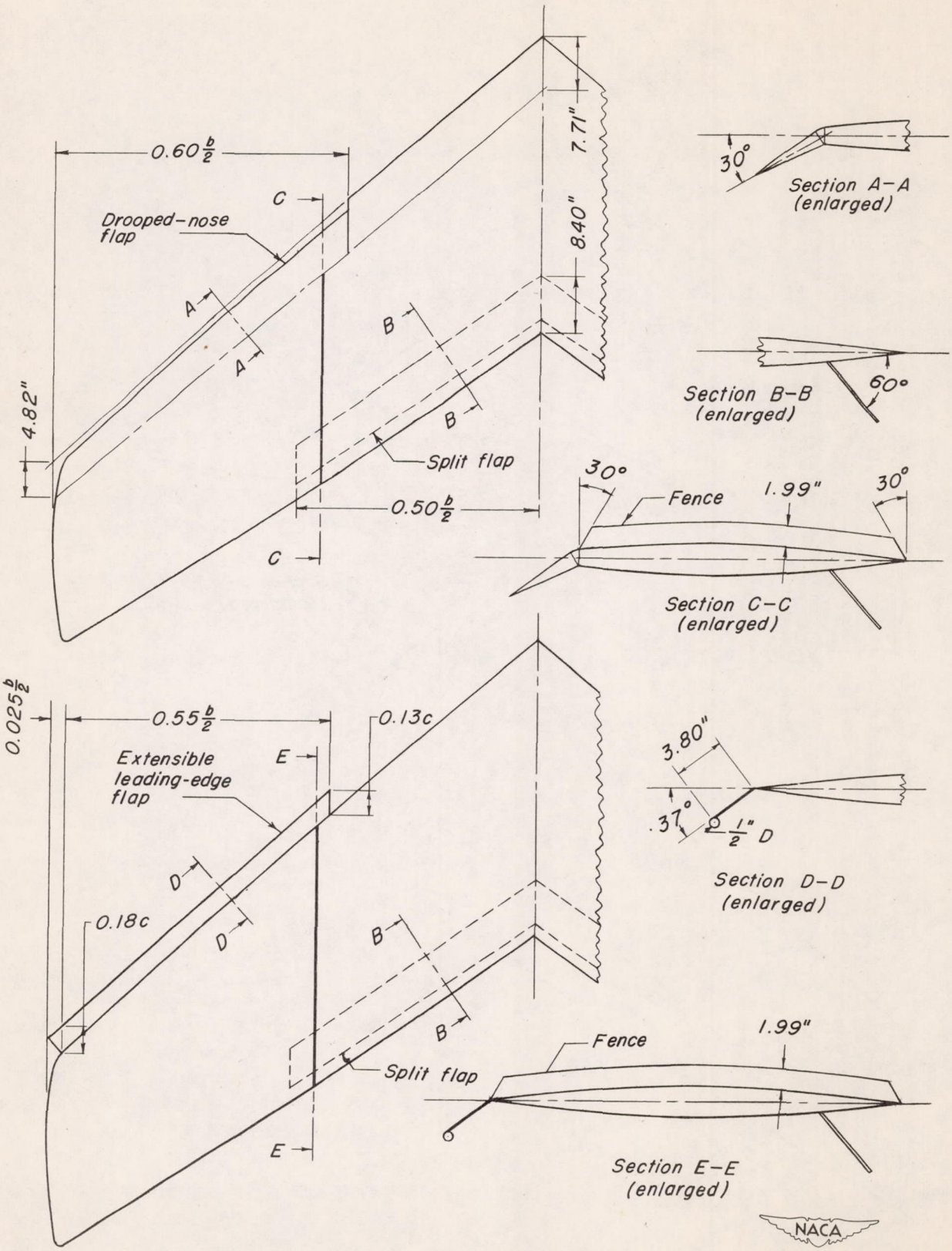

Figure 3.- Details of high-lift and stall-control devices.

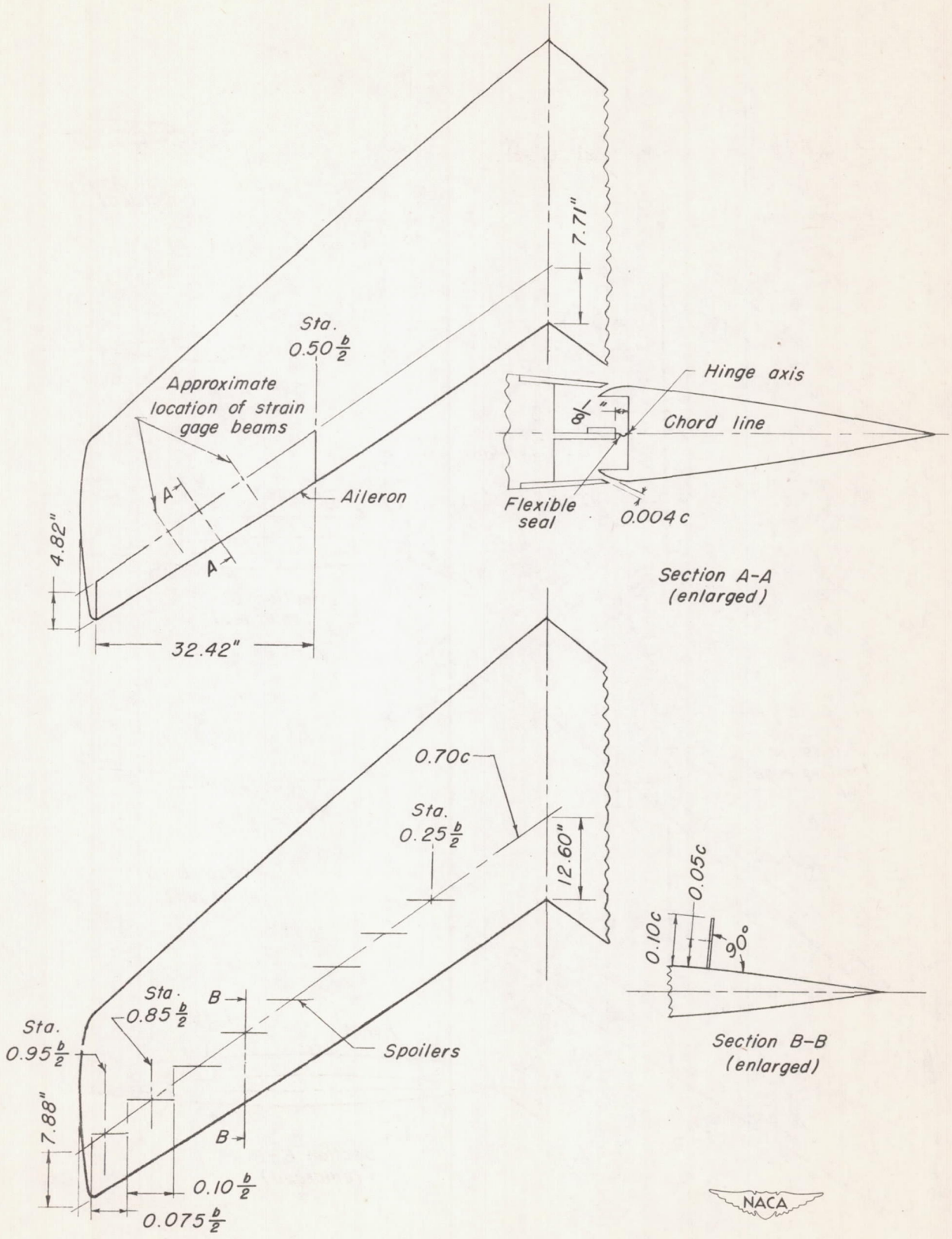

Figure 4.– Geometry of aileron and spoilers.

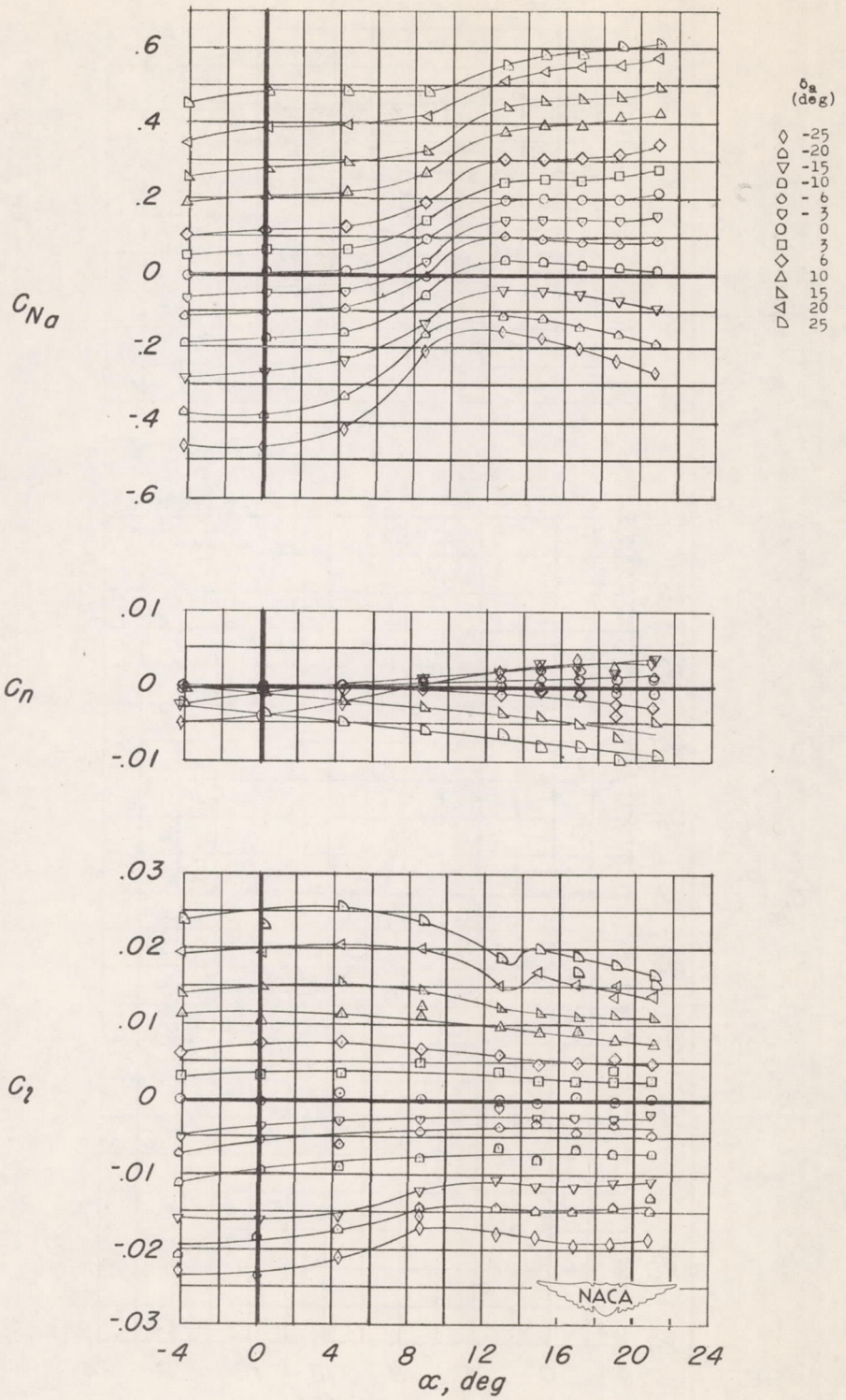

(a) C_l, C_n, and C_{N_a} against α.

Figure 5.– Aileron characteristics of plain wing.

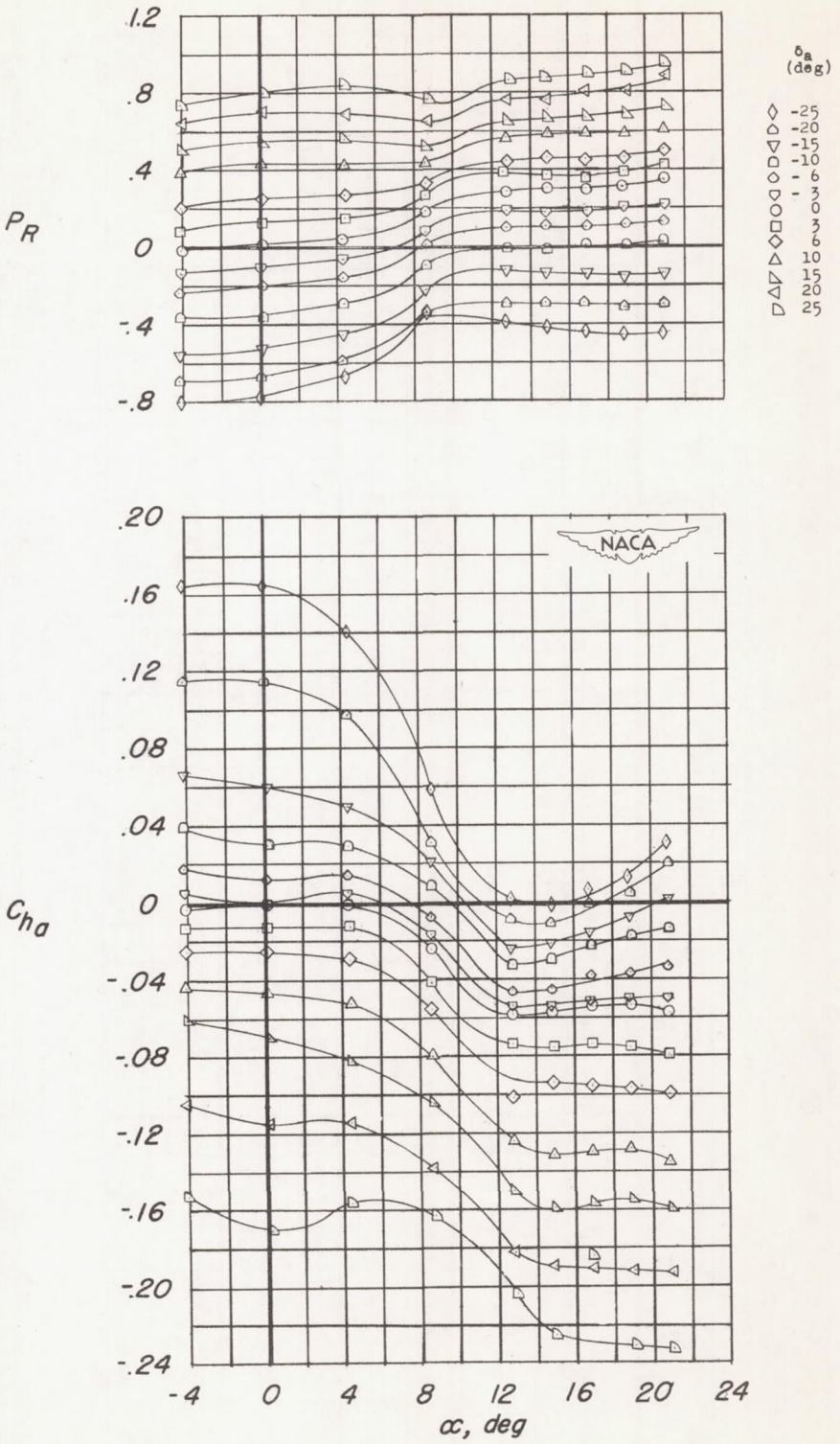

(b) C_{h_a} and P_R against α.

Figure 5.– Continued.

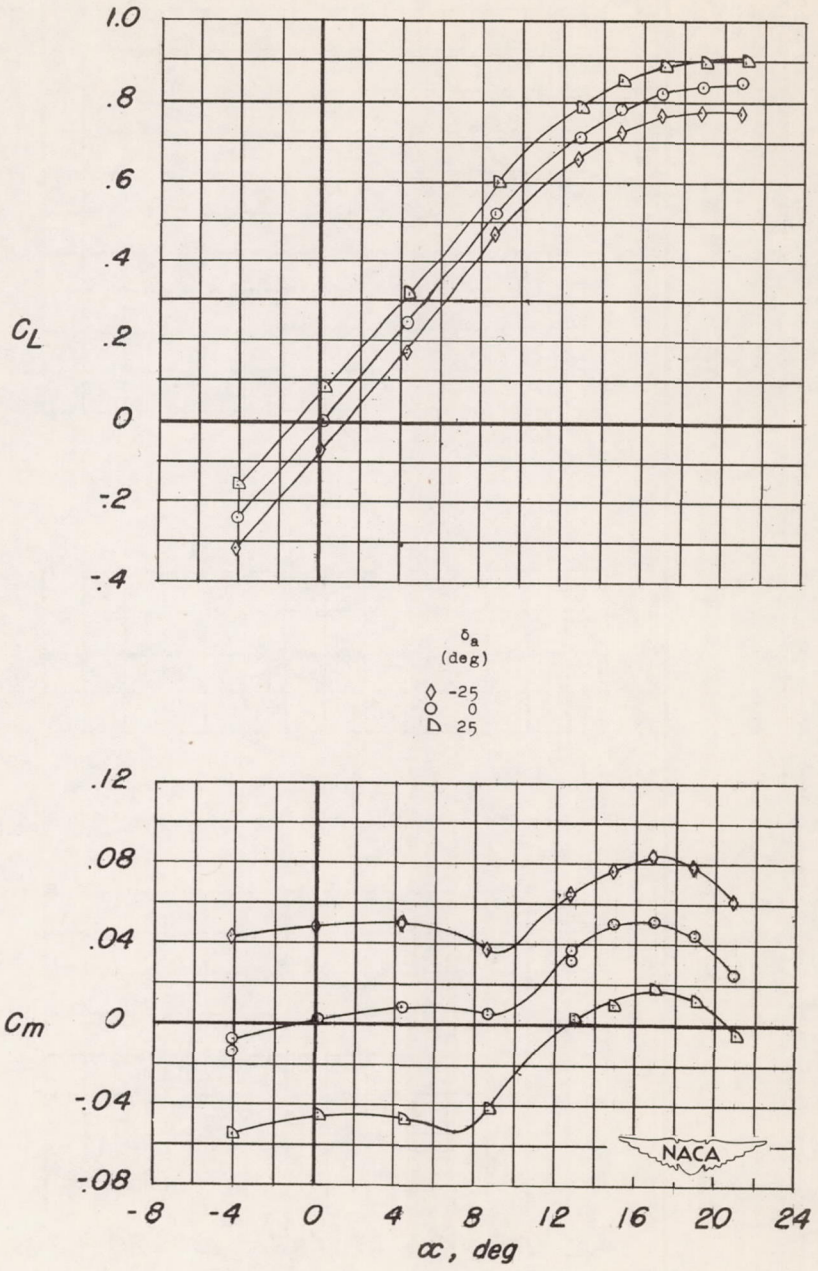

(c) C_L and C_m against α.

Figure 5.– Concluded.

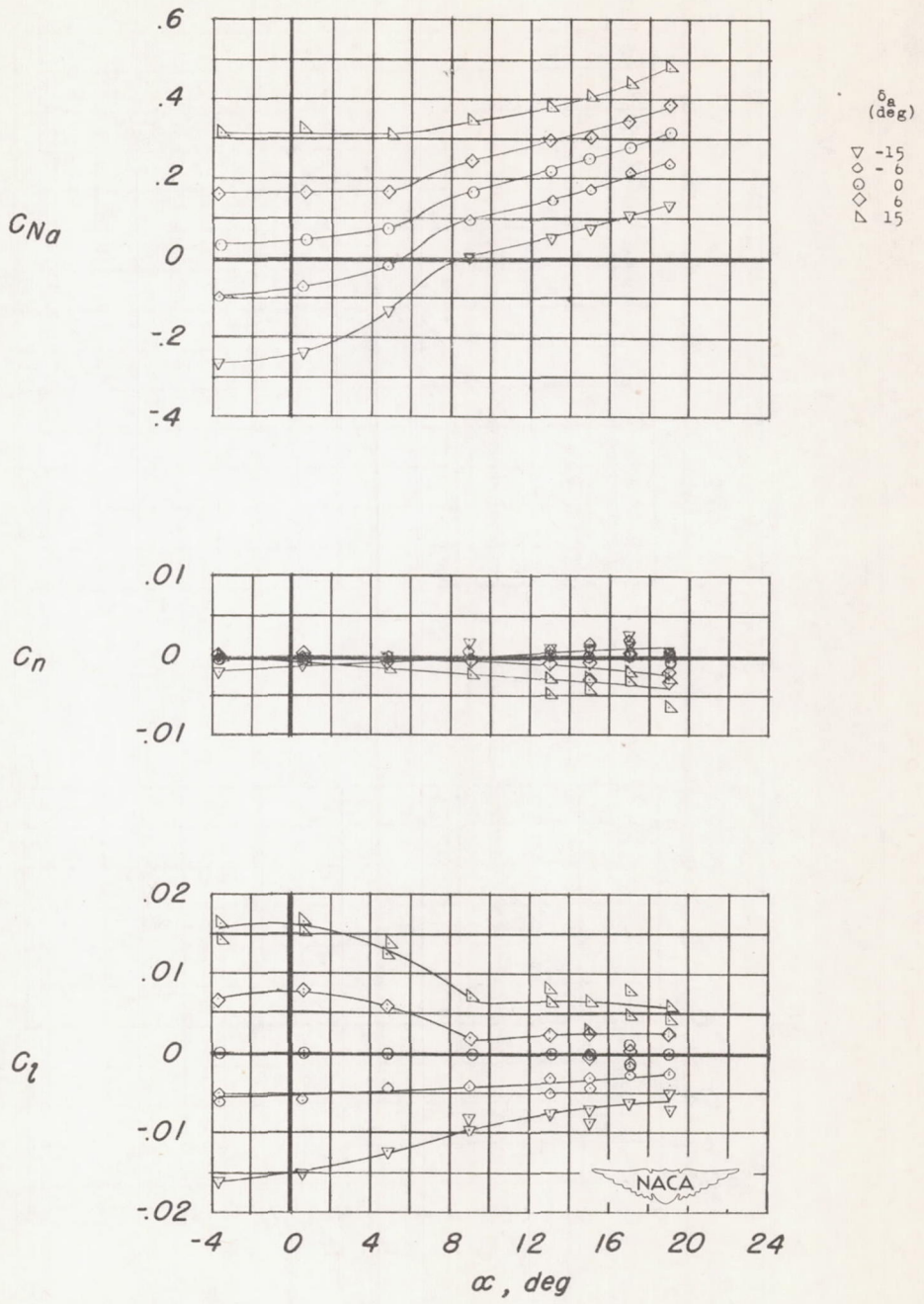

(a) C_l, C_n, and C_{N_a} against α.

Figure 6.– Aileron characteristics of wing with split flaps.

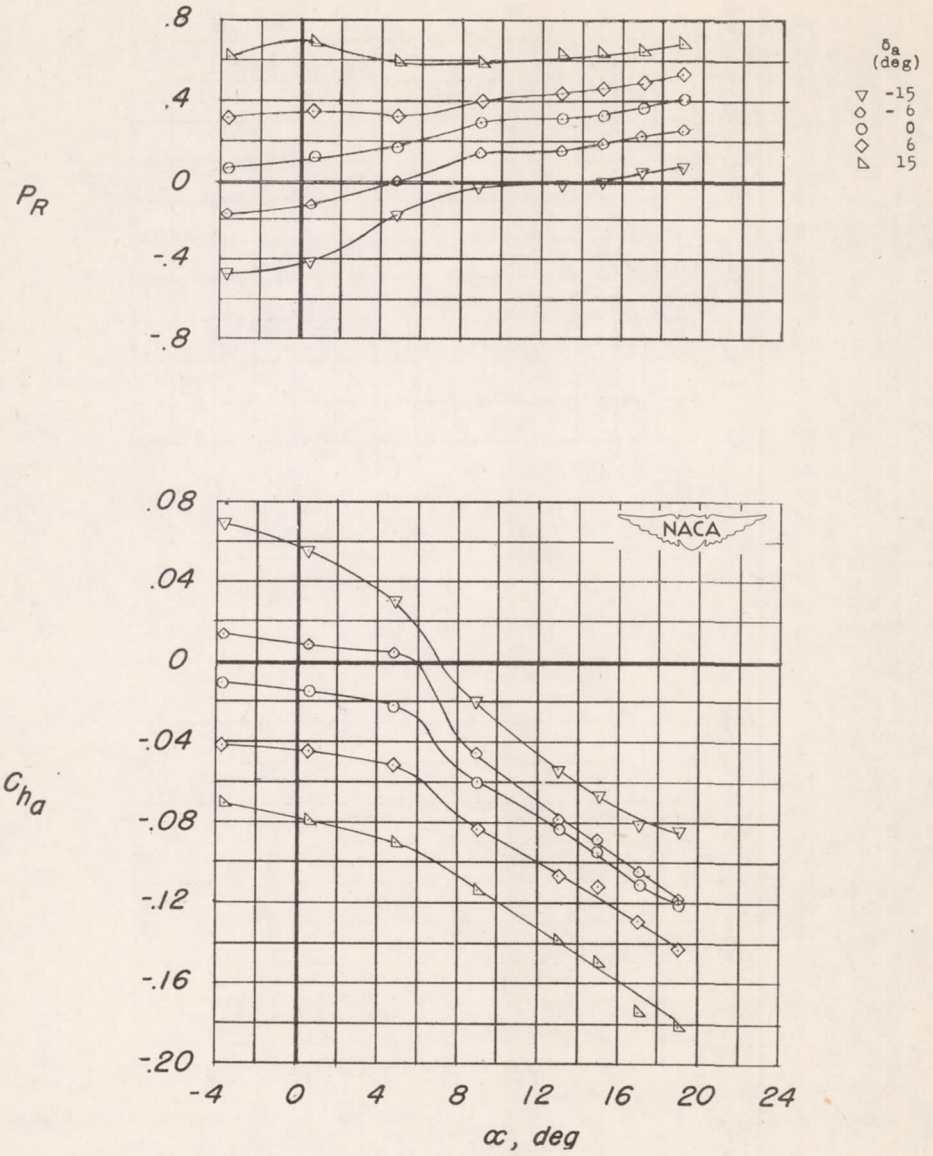

(b) C_{h_a} and P_R against α.

Figure 6.– Continued.

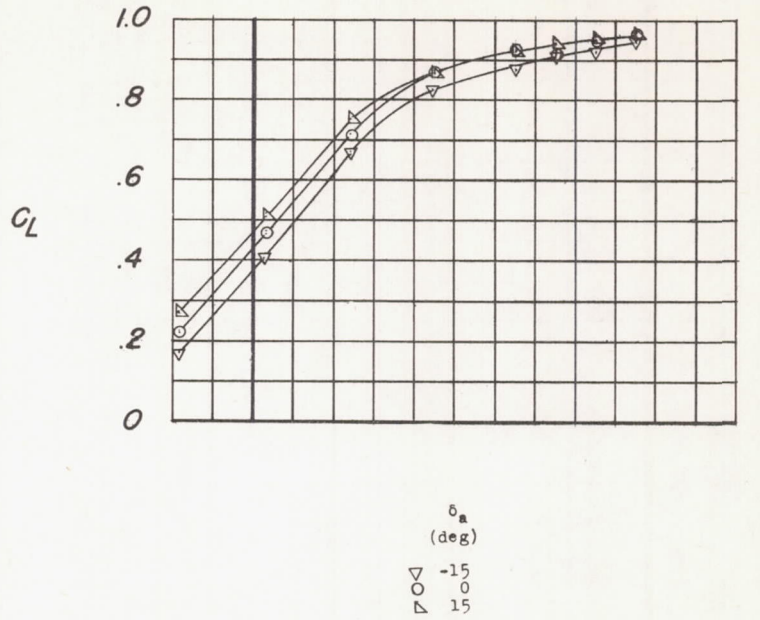

(c) C_L and C_m against α.

Figure 6.– Concluded.

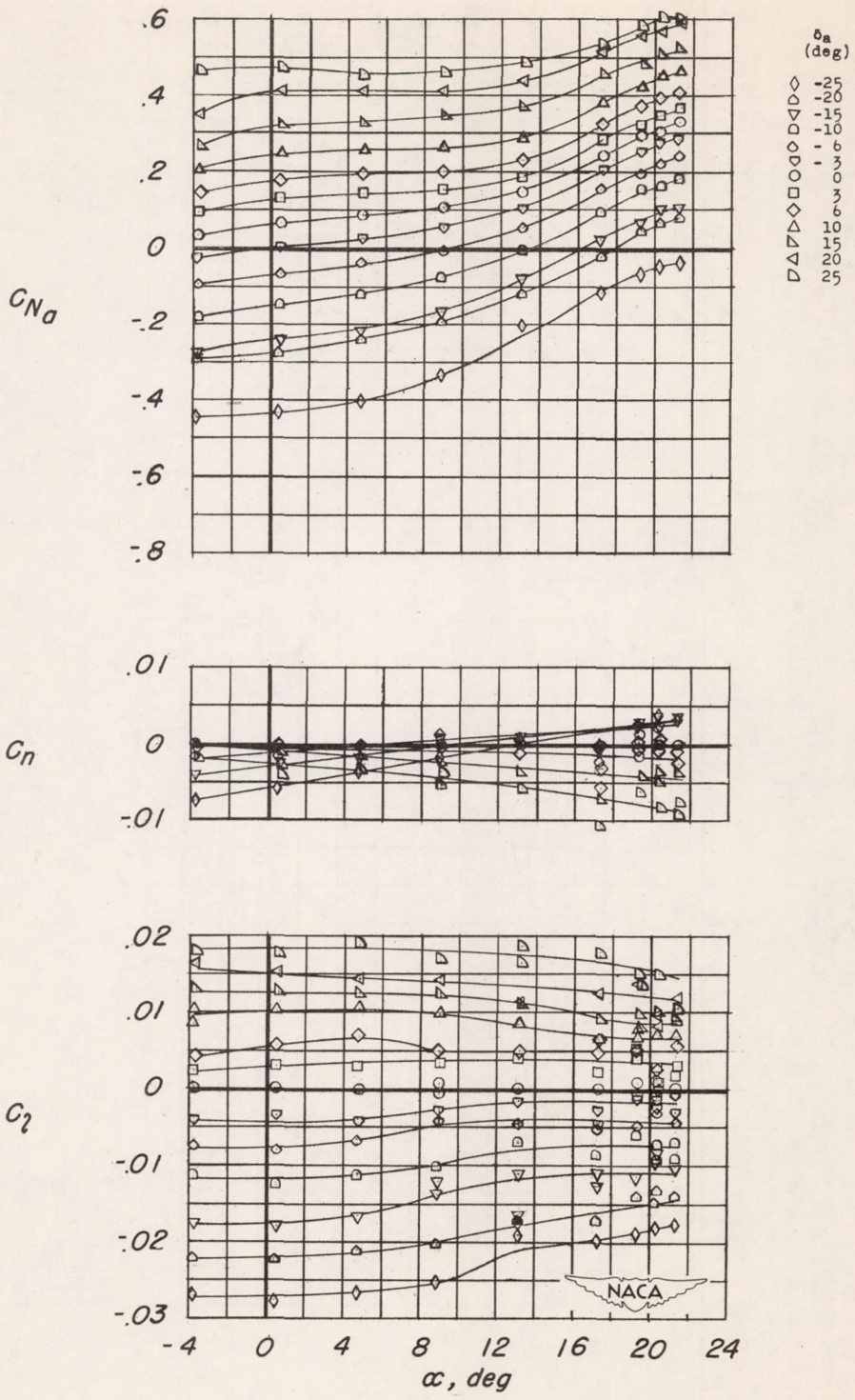

(a) C_l, C_n, and C_{N_a} against α.

Figure 7.– Aileron characteristics of wing with drooped–nose and split flaps and fences.

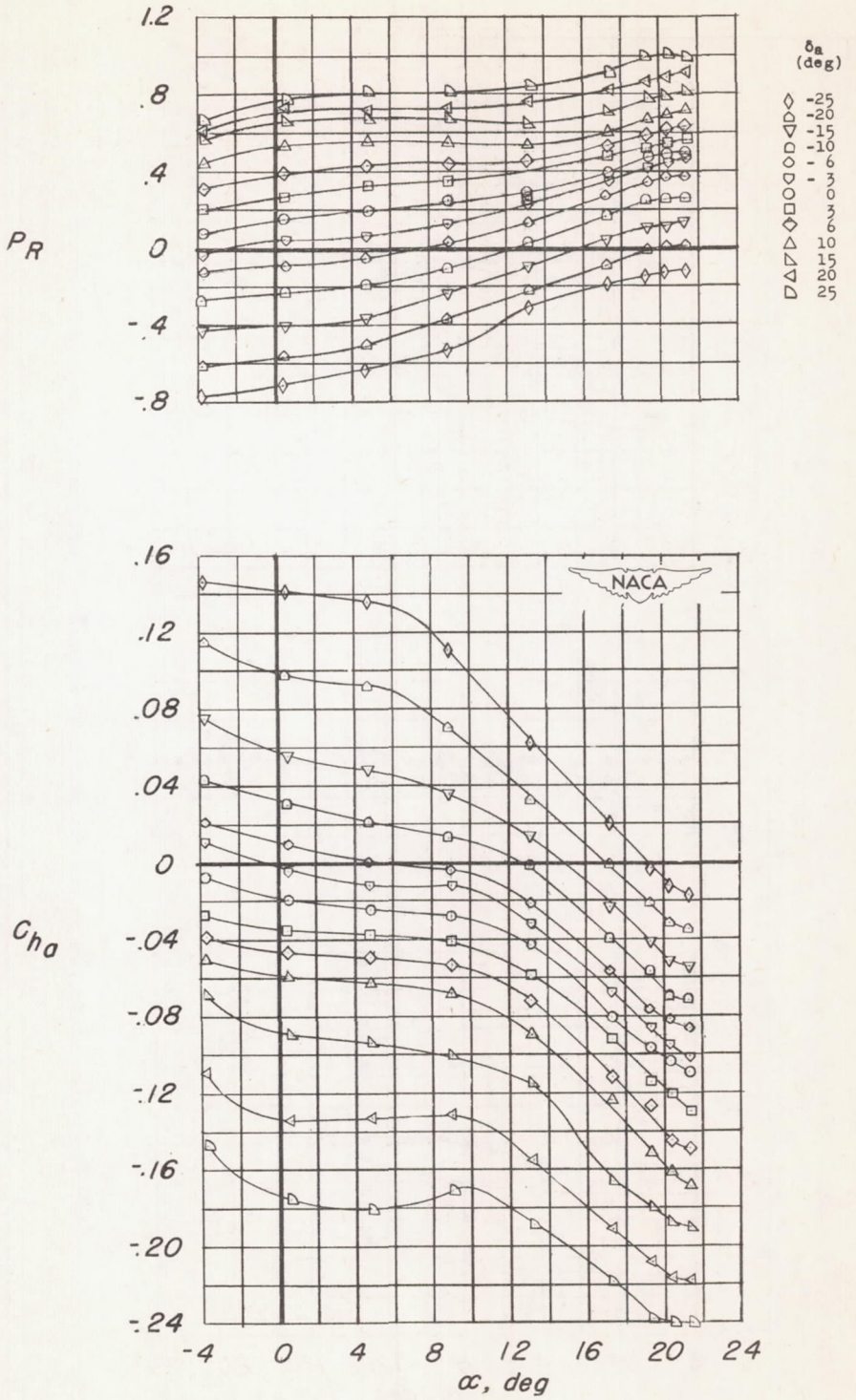

(b) C_{h_a} and P_R against α.

Figure 7.- Continued.

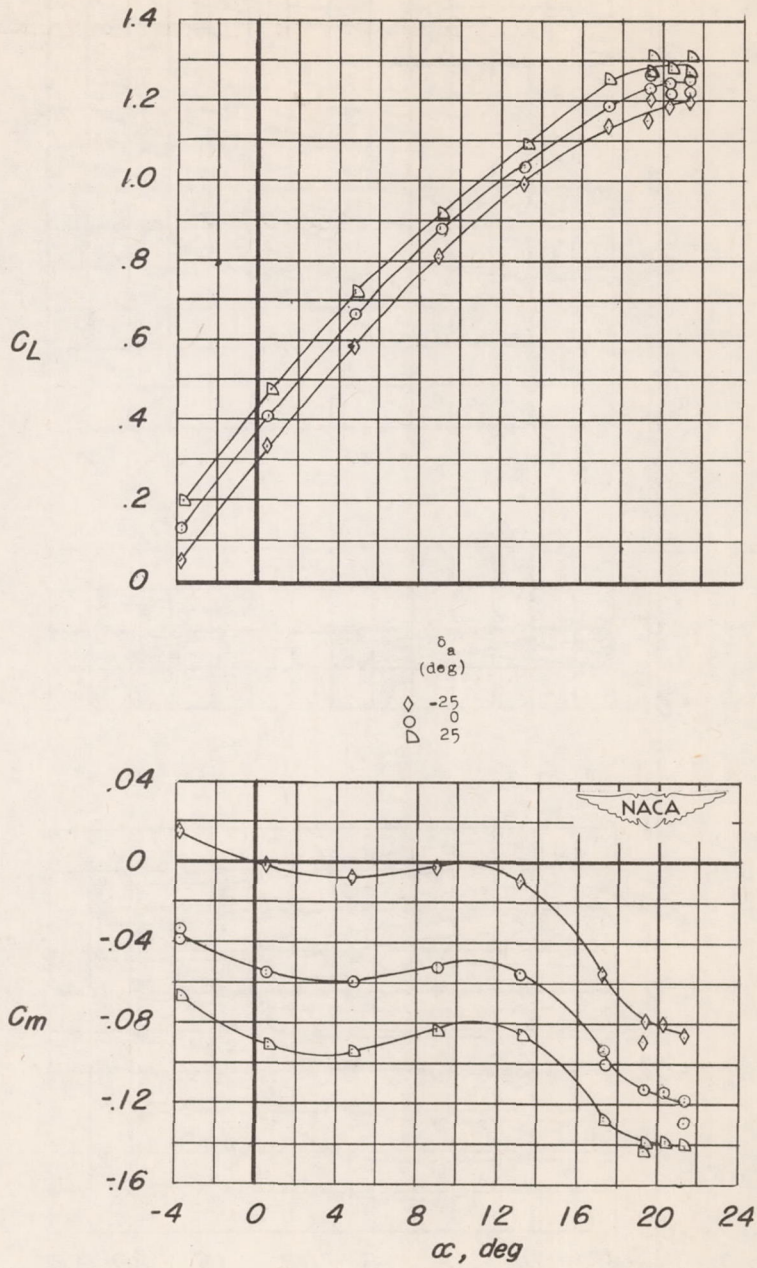

(c) C_L and C_m against α.

Figure 7.– Concluded.

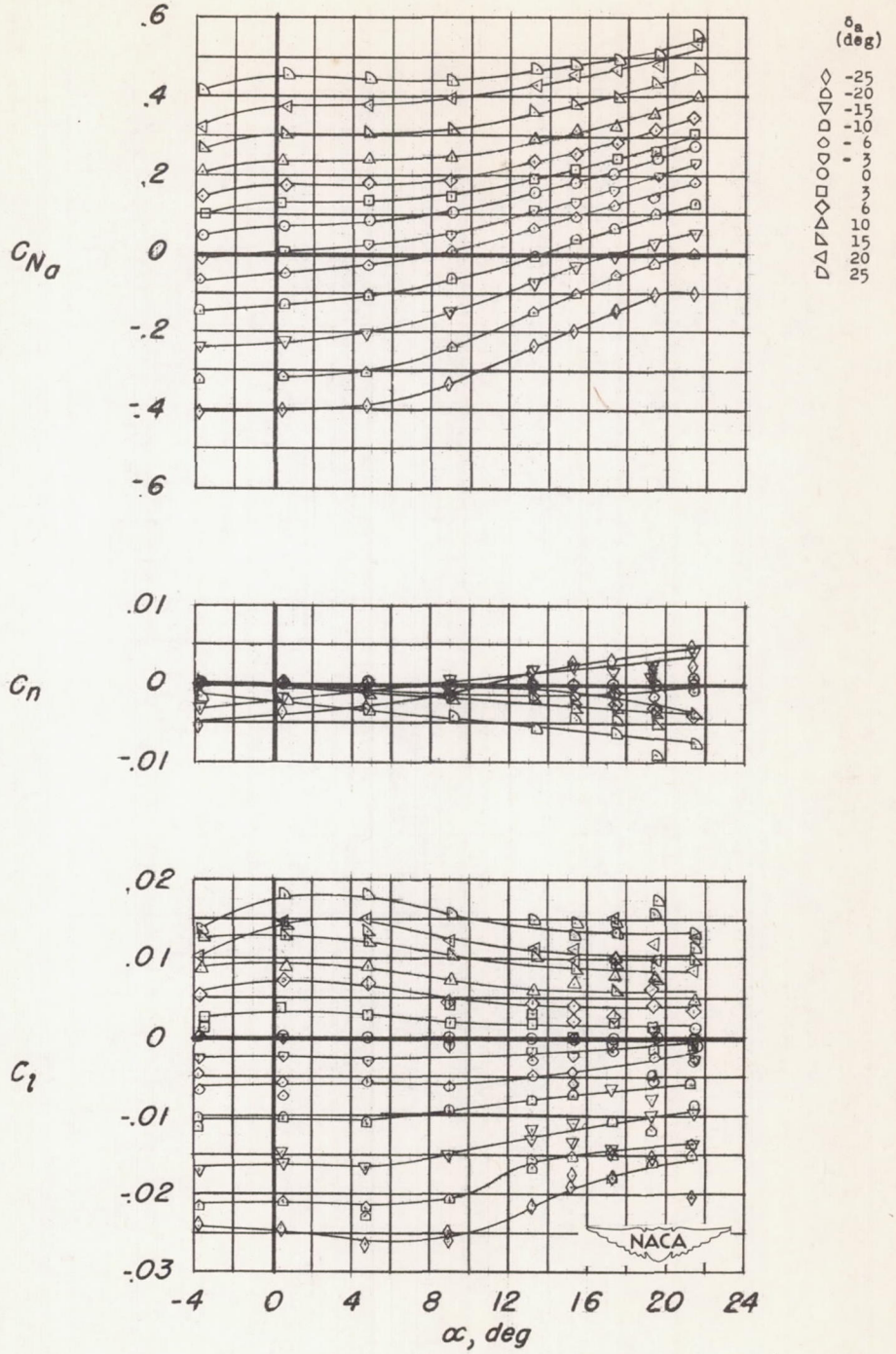

(a) C_l, C_n, and C_{N_a} against α.

Figure 8.– Aileron characteristics of wing with extensible leading–edge and split flaps.

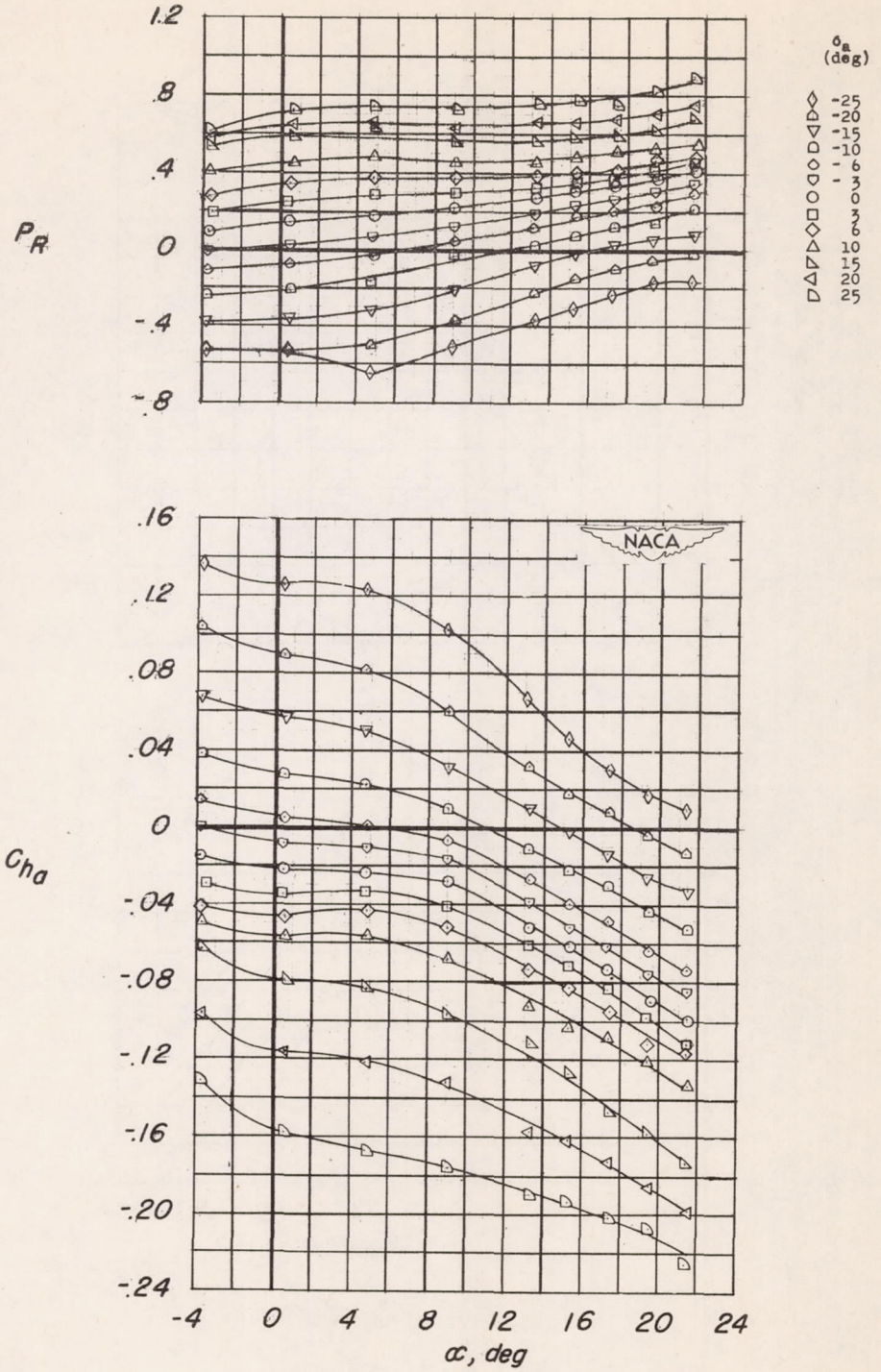

(b) C_{h_a} and P_R against α.

Figure 8.– Continued.

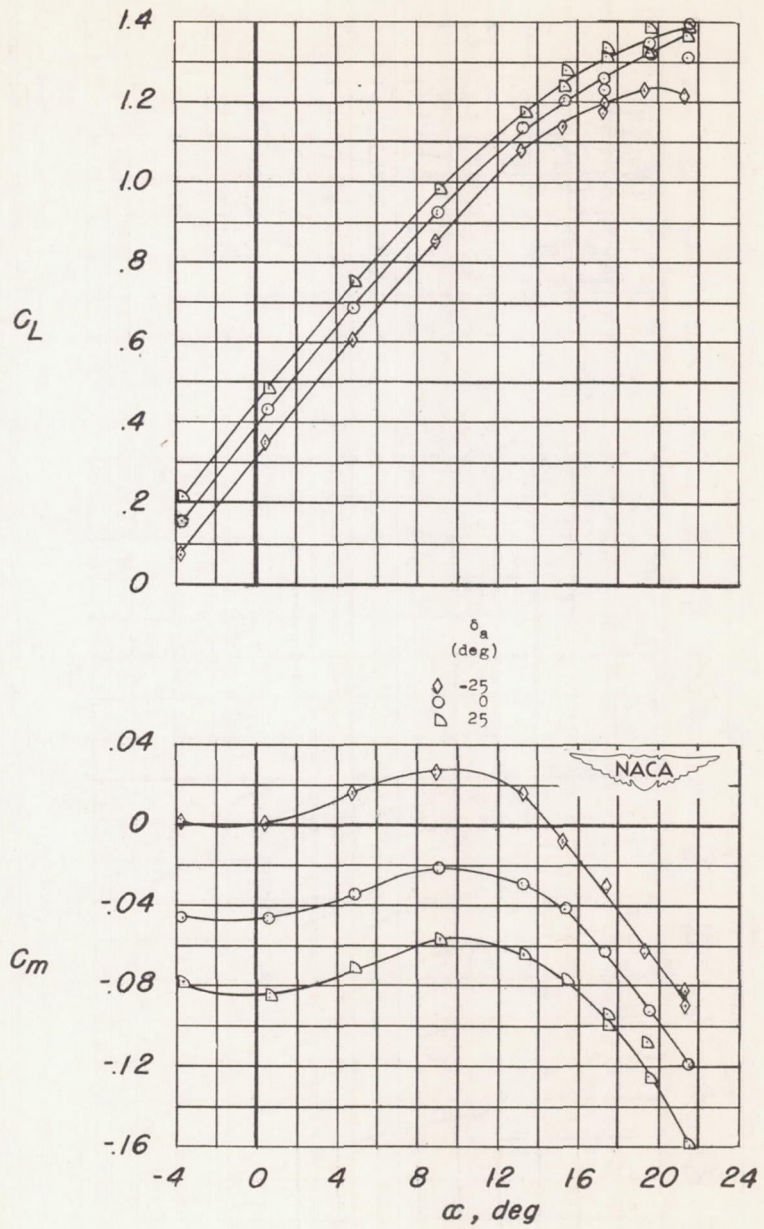

(c) C_L and C_m against α.

Figure 8.– Concluded.

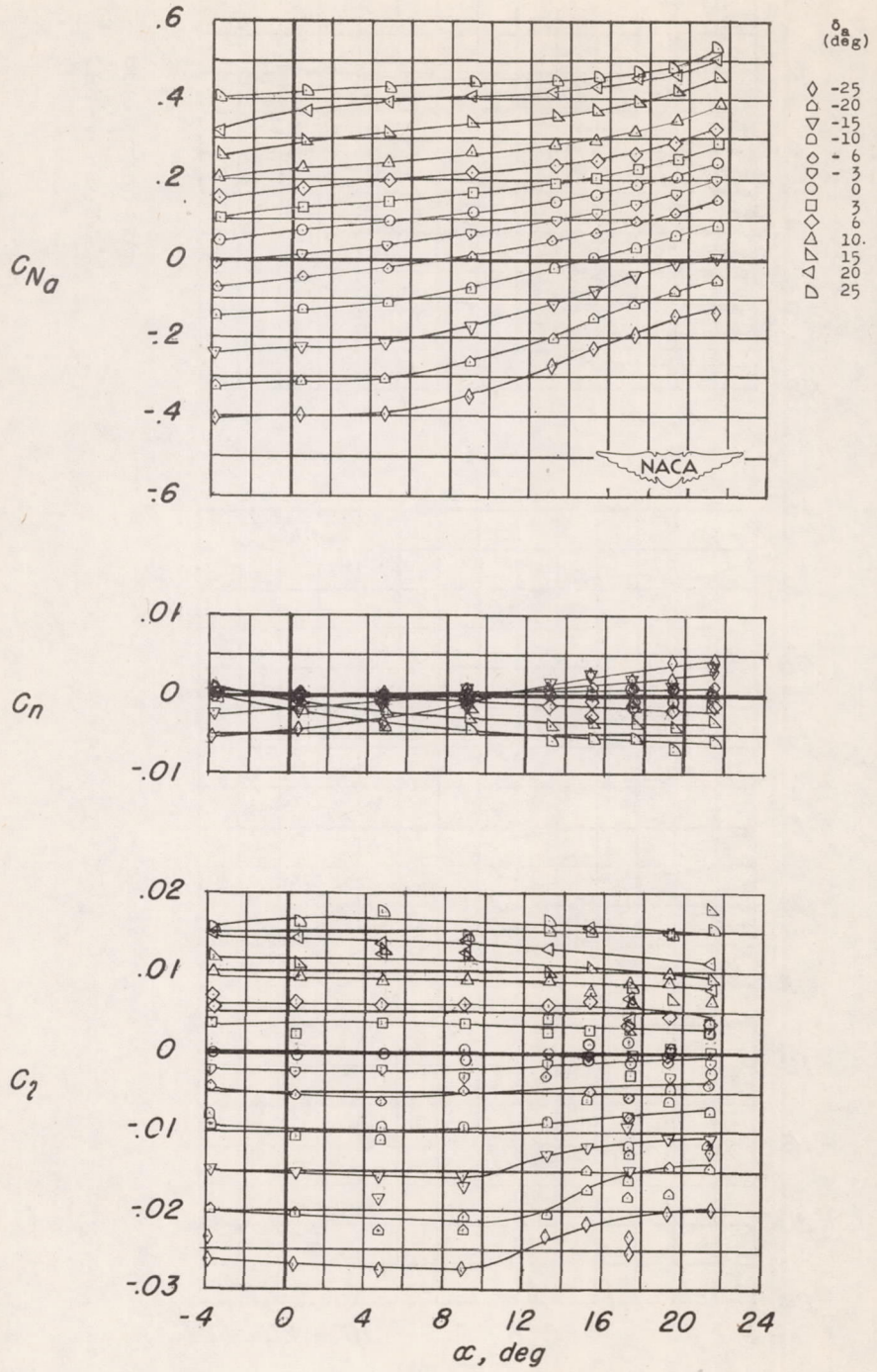

(a) C_l, C_n, and C_{N_a} against α.

Figure 9.– Aileron characteristics of wing with extensible leading–edge and split flaps and fences.

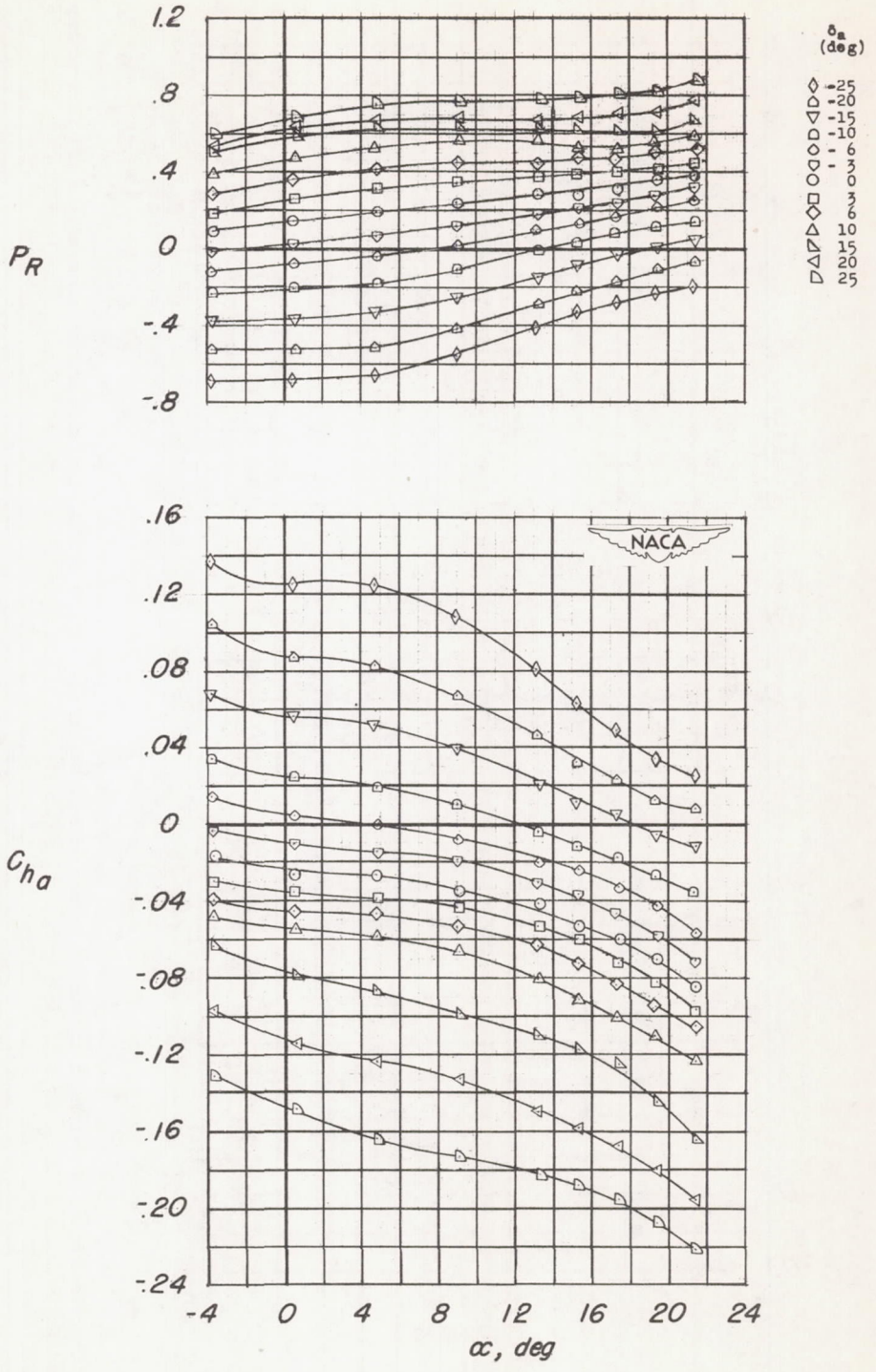

(b) C_{h_a} and P_R against α.

Figure 9.- Continued.

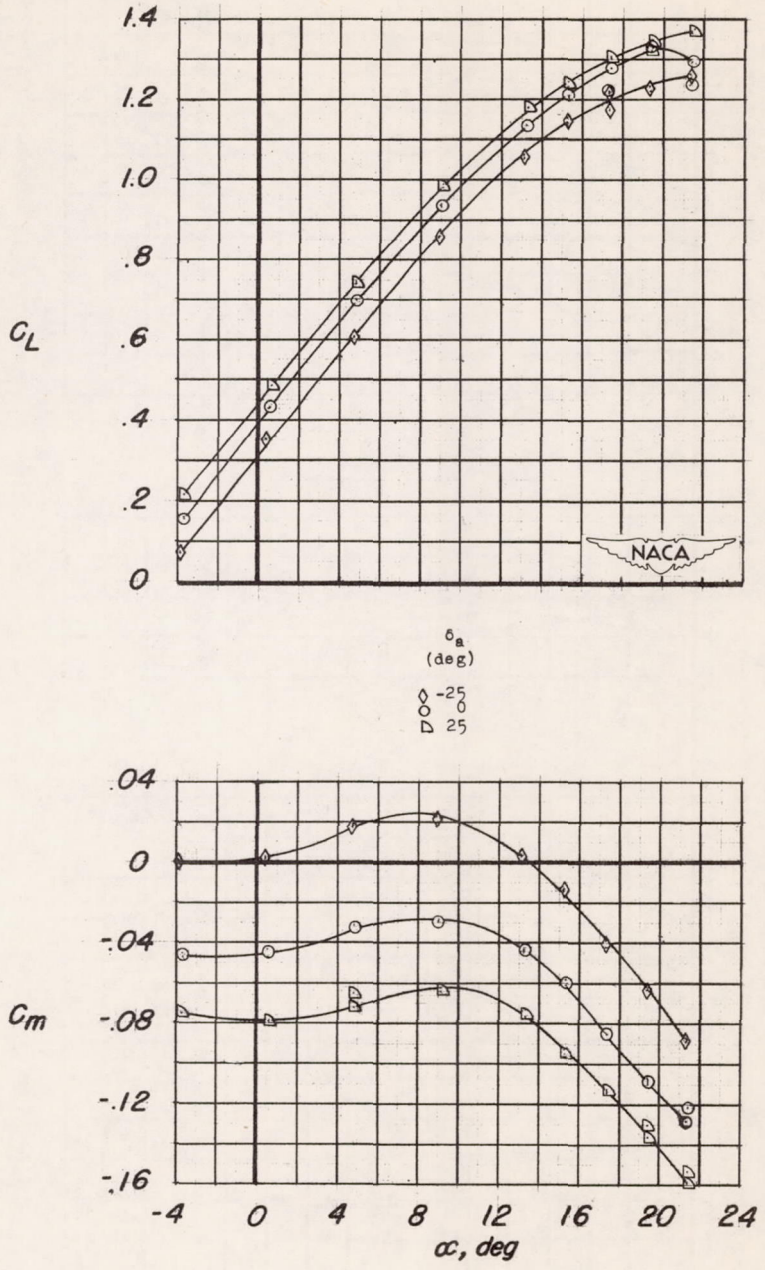

(c) C_L and C_m against α.

Figure 9.– Concluded.

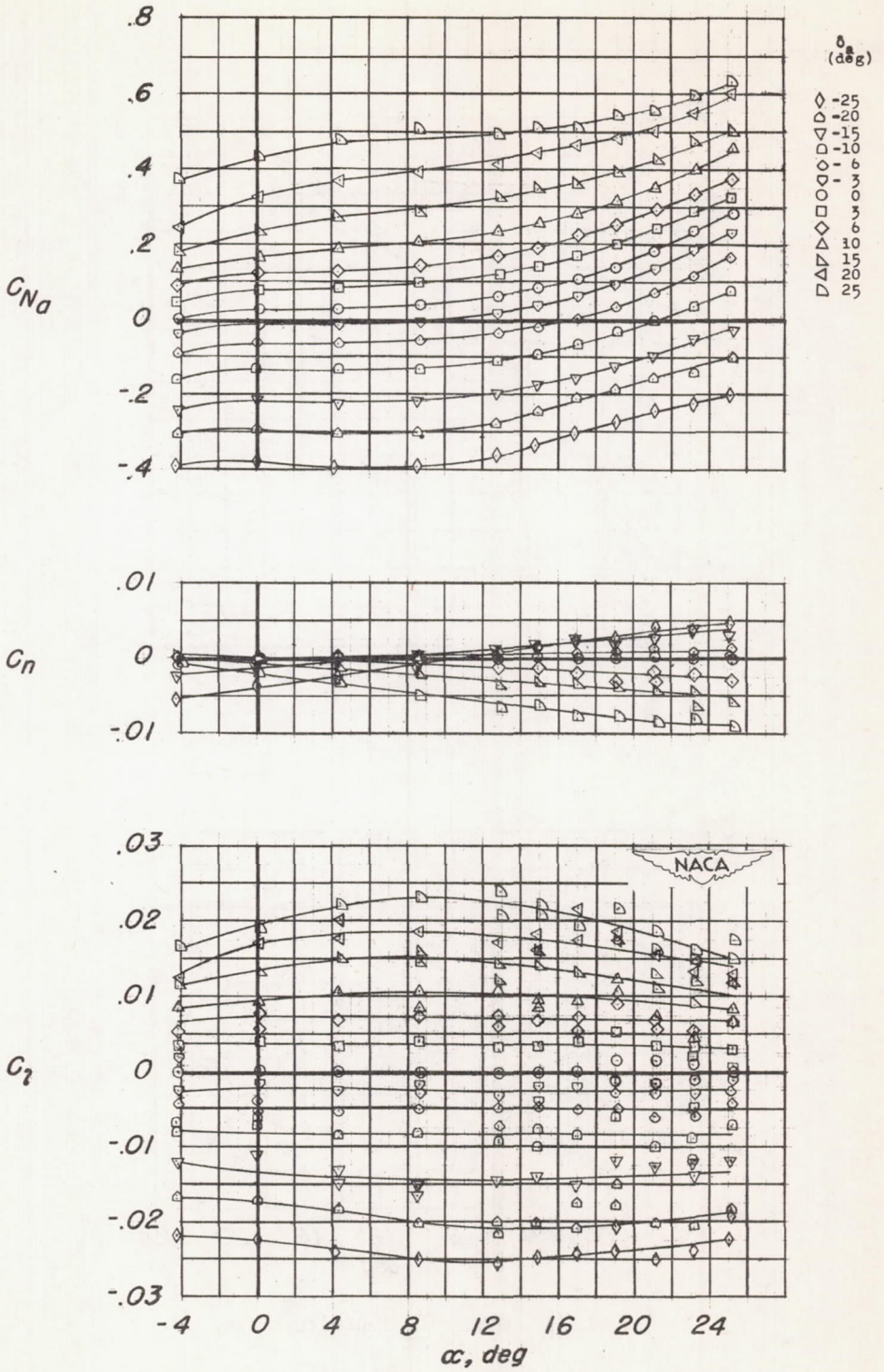

(a) C_l, C_n, and C_{N_a} against α.

Figure 10.– Aileron characteristics of wing with extensible leading-edge flaps and fences.

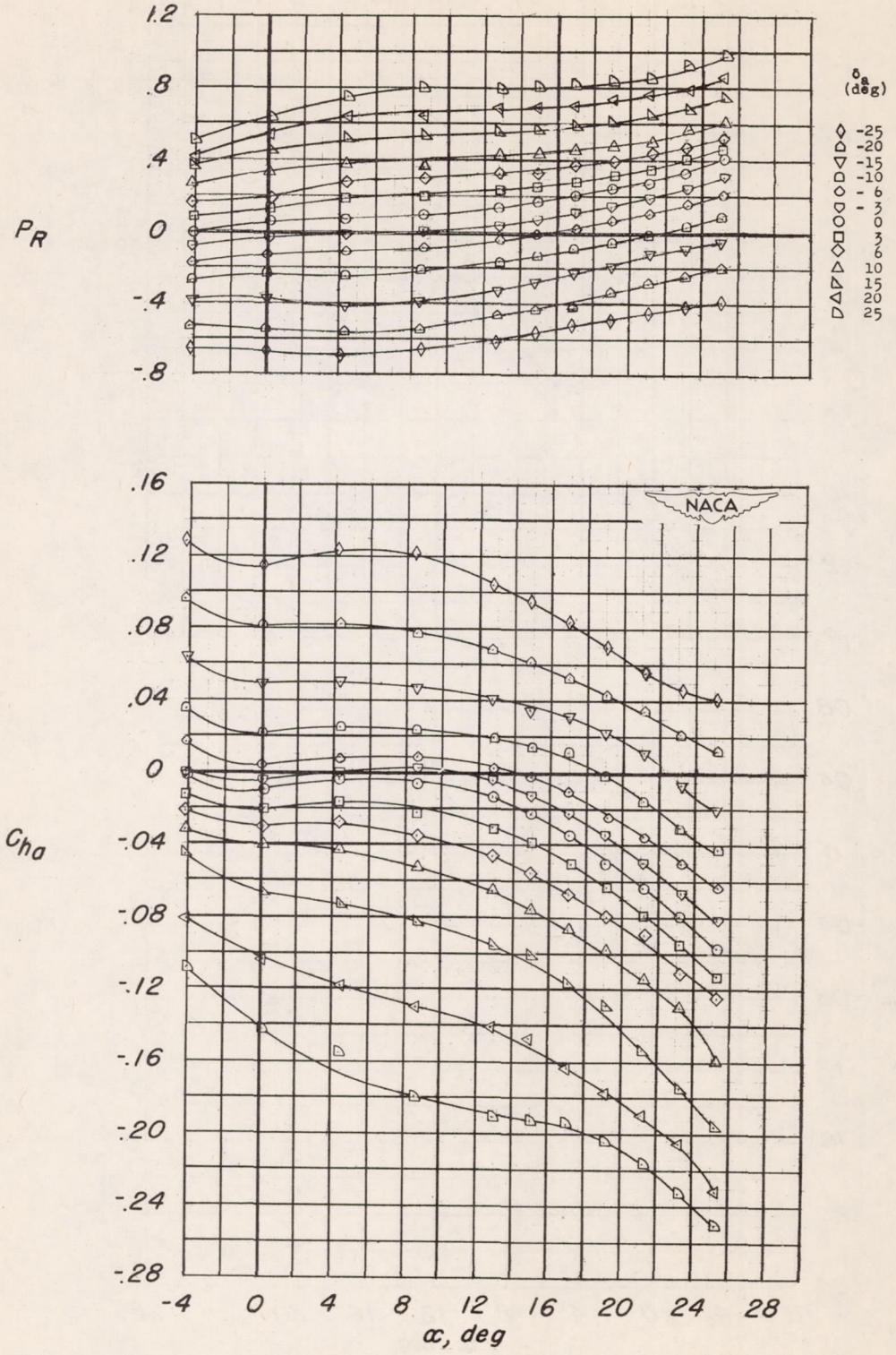

(b) C_{h_a} and P_R against α.

Figure 10.– Continued.

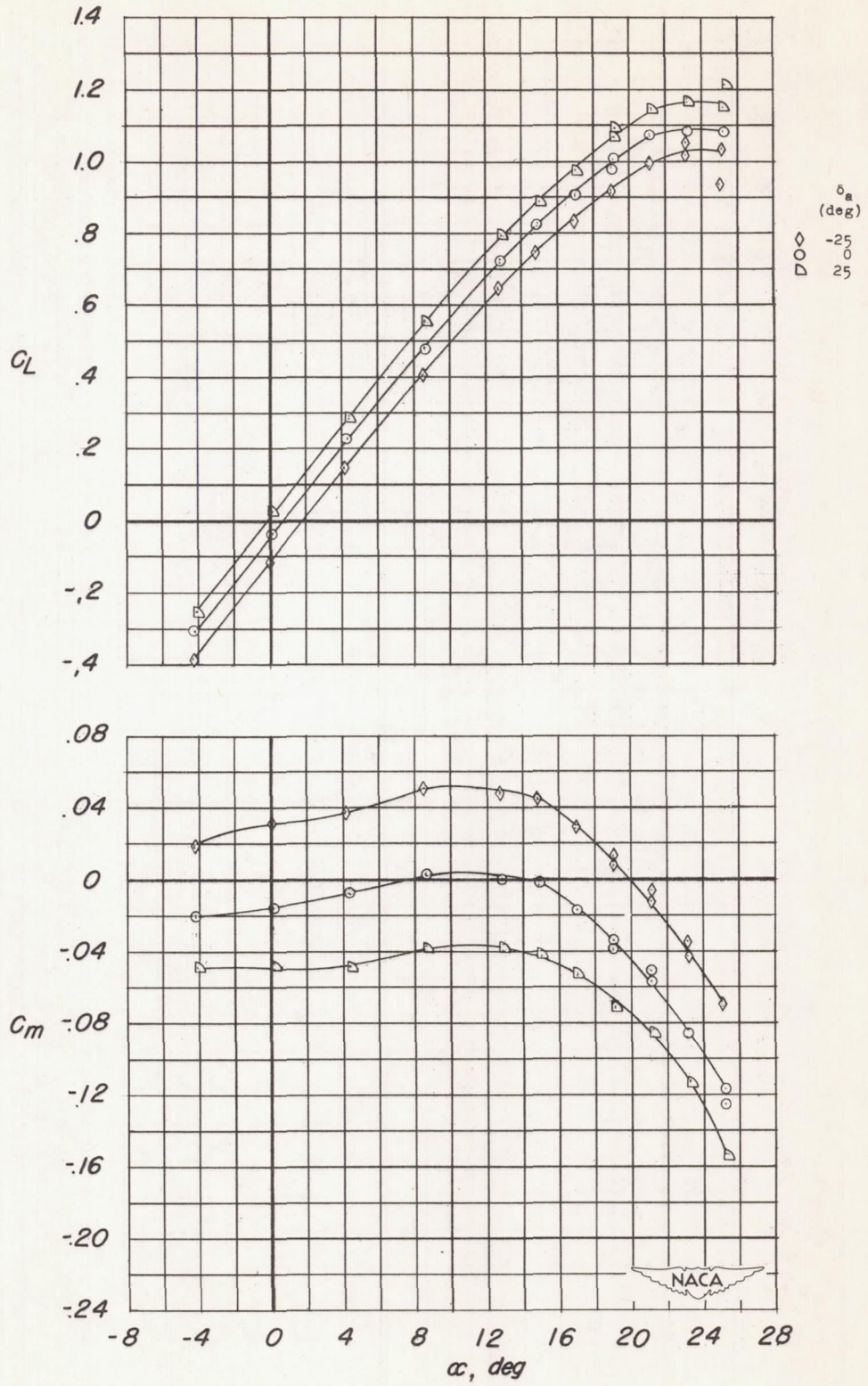

(c) C_L and C_m against α.

Figure 10.– Concluded.

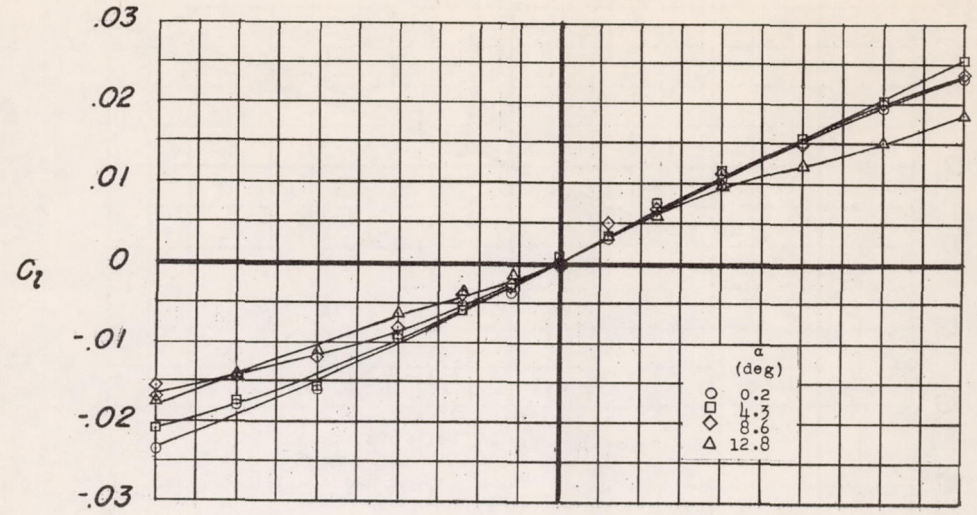

(a) Plain wing

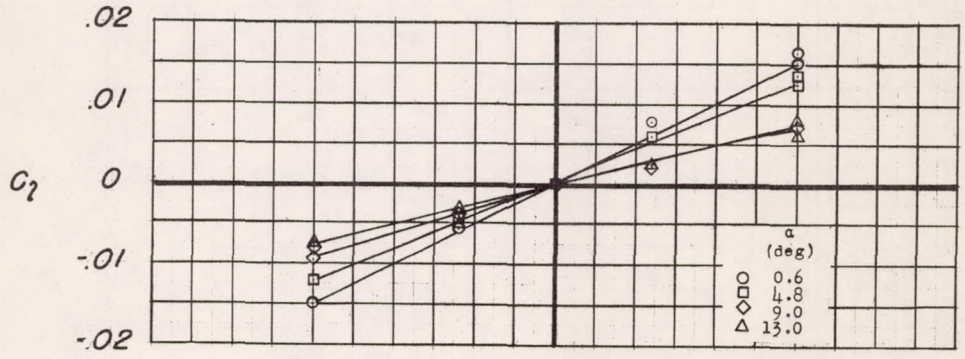

(b) Split flaps

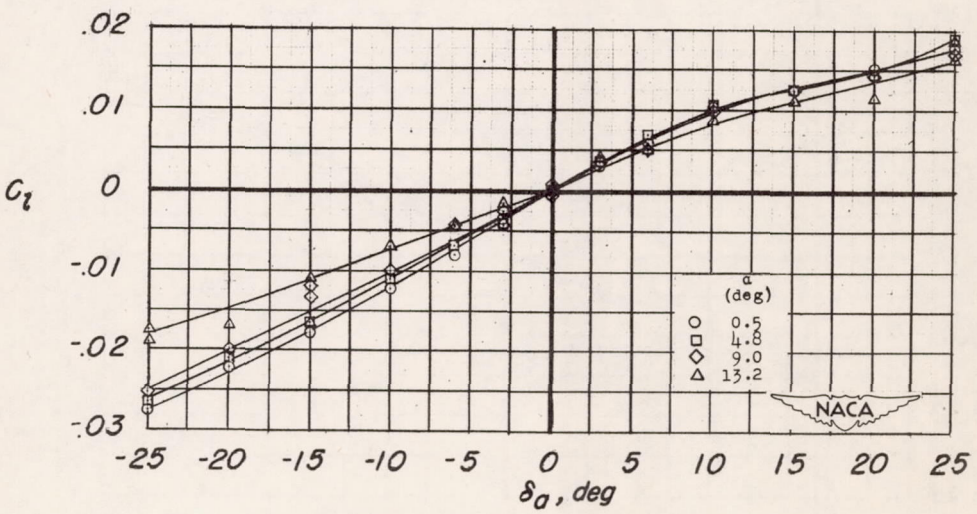

(c) Drooped-nose and split flaps and fences.

Figure 11.– Variation of rolling-moment coefficient with aileron deflection for various flap configurations.

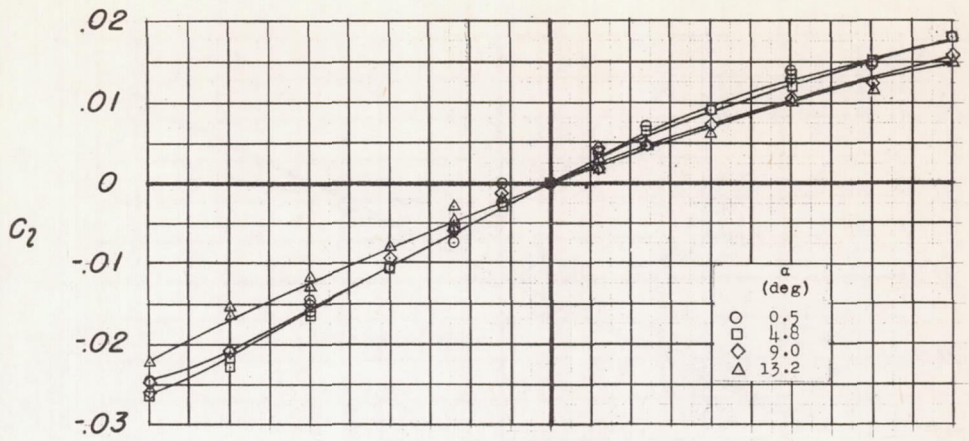

(d) Leading-edge and split flaps.

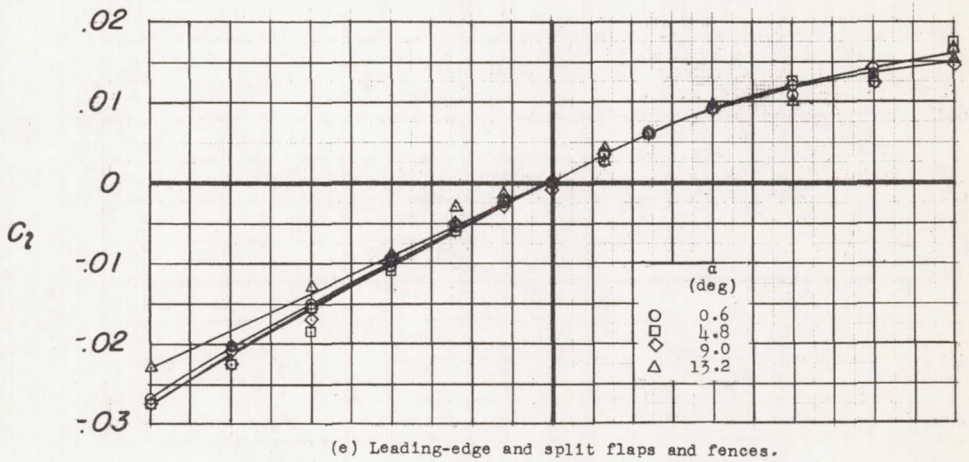

(e) Leading-edge and split flaps and fences.

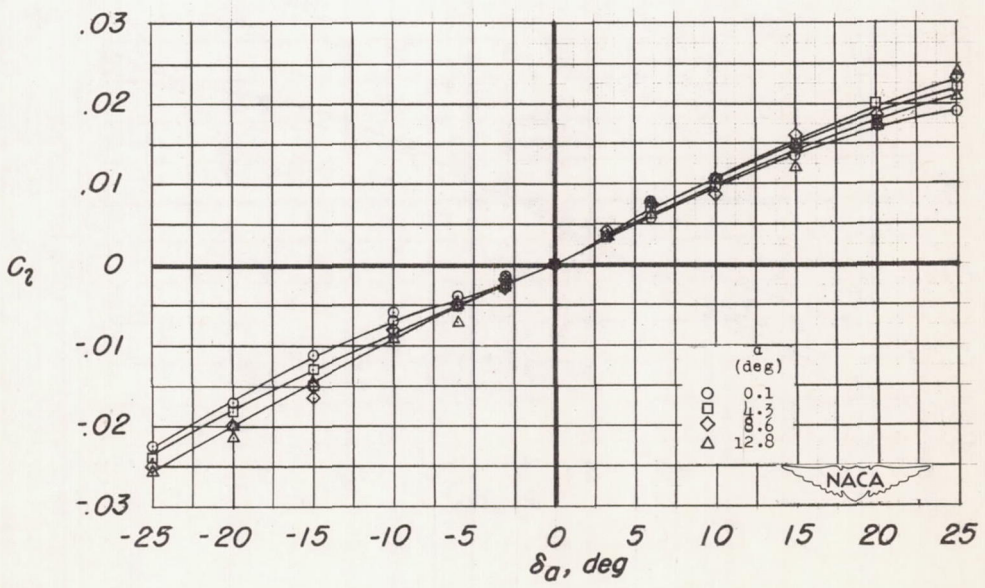

(f) Leading-edge flaps and fences.

Figure 11.– Concluded.

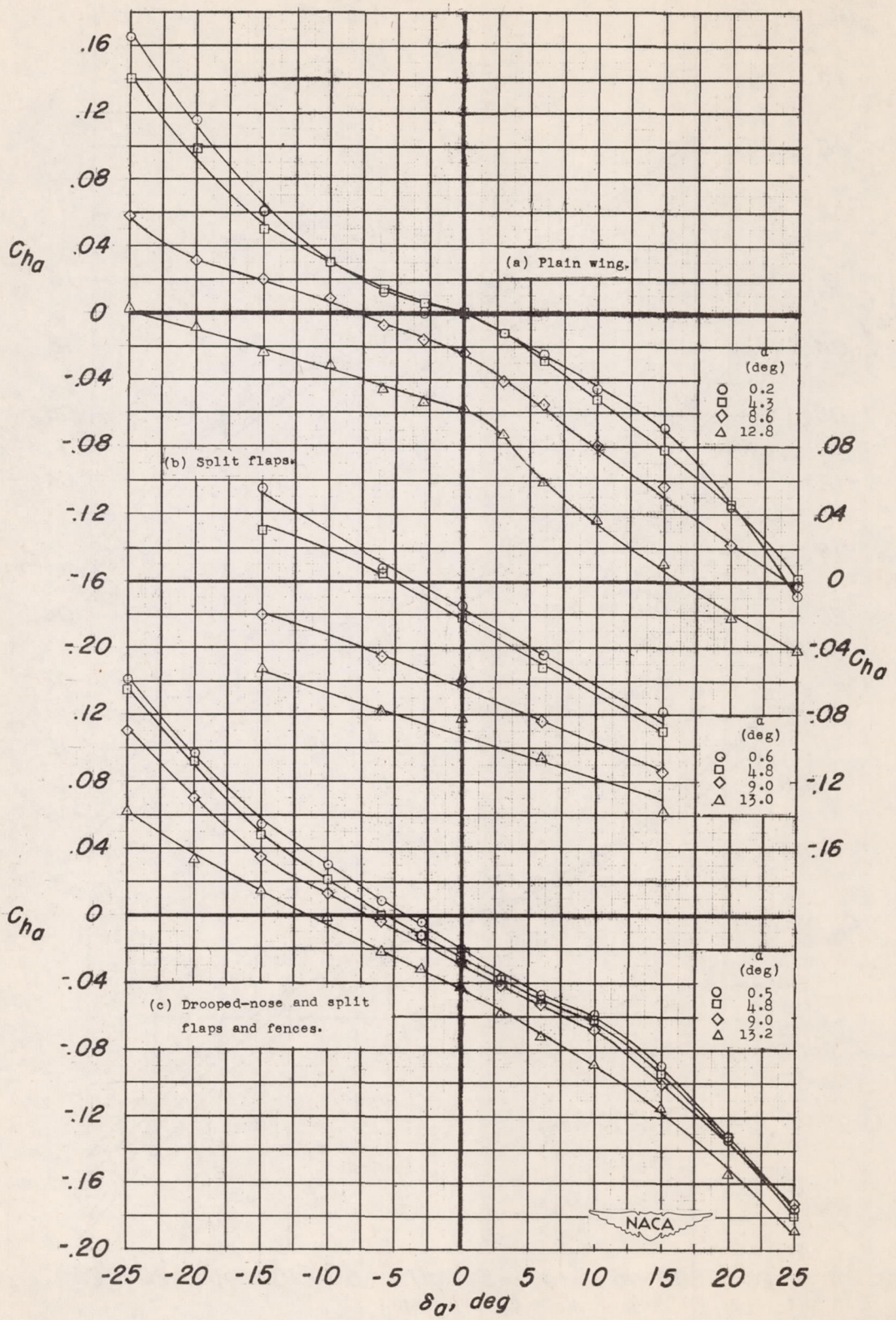

Figure 12.– Variation of aileron hinge–moment coefficient with aileron deflection for various flap configurations.

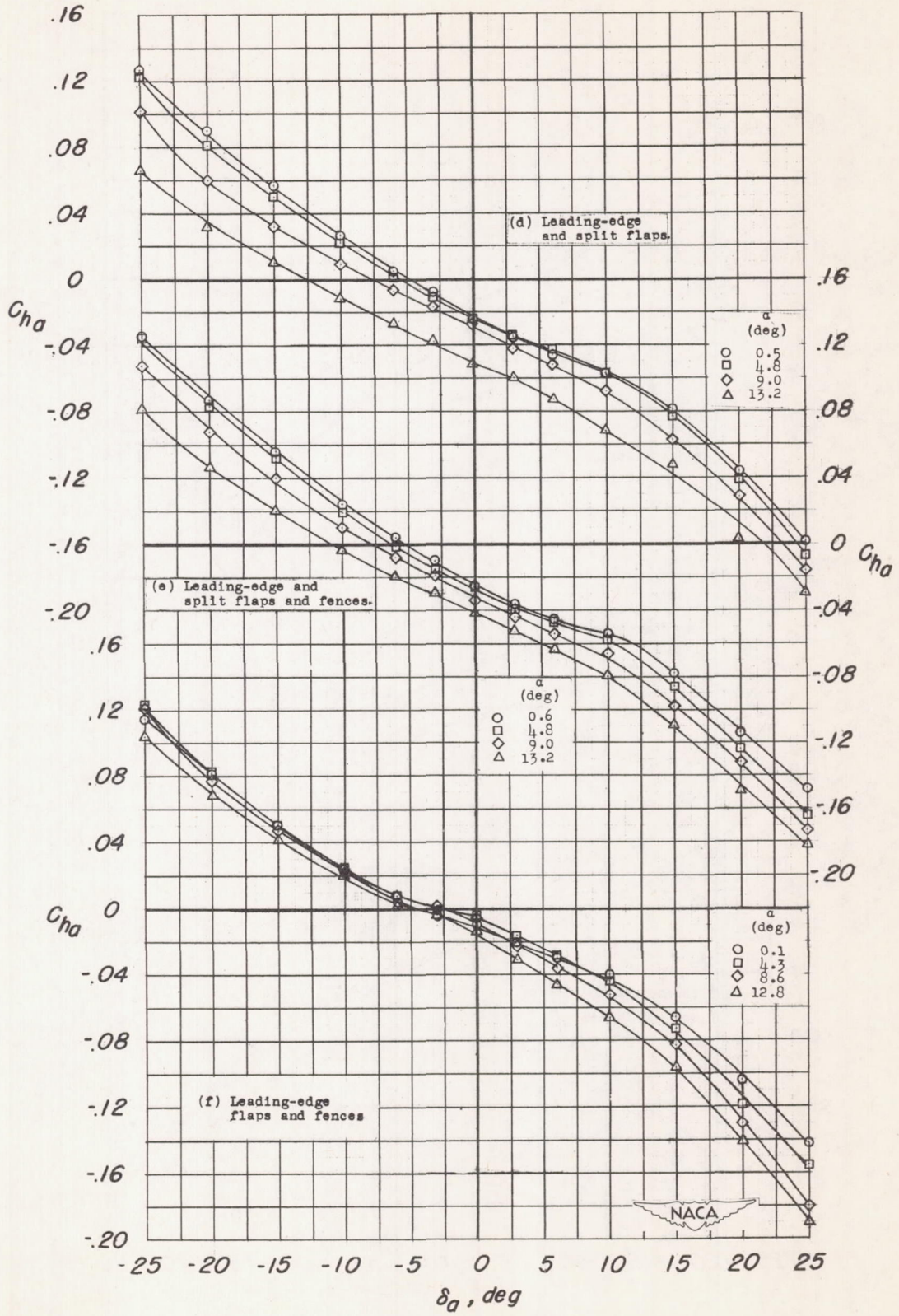

Figure 12.– Concluded.

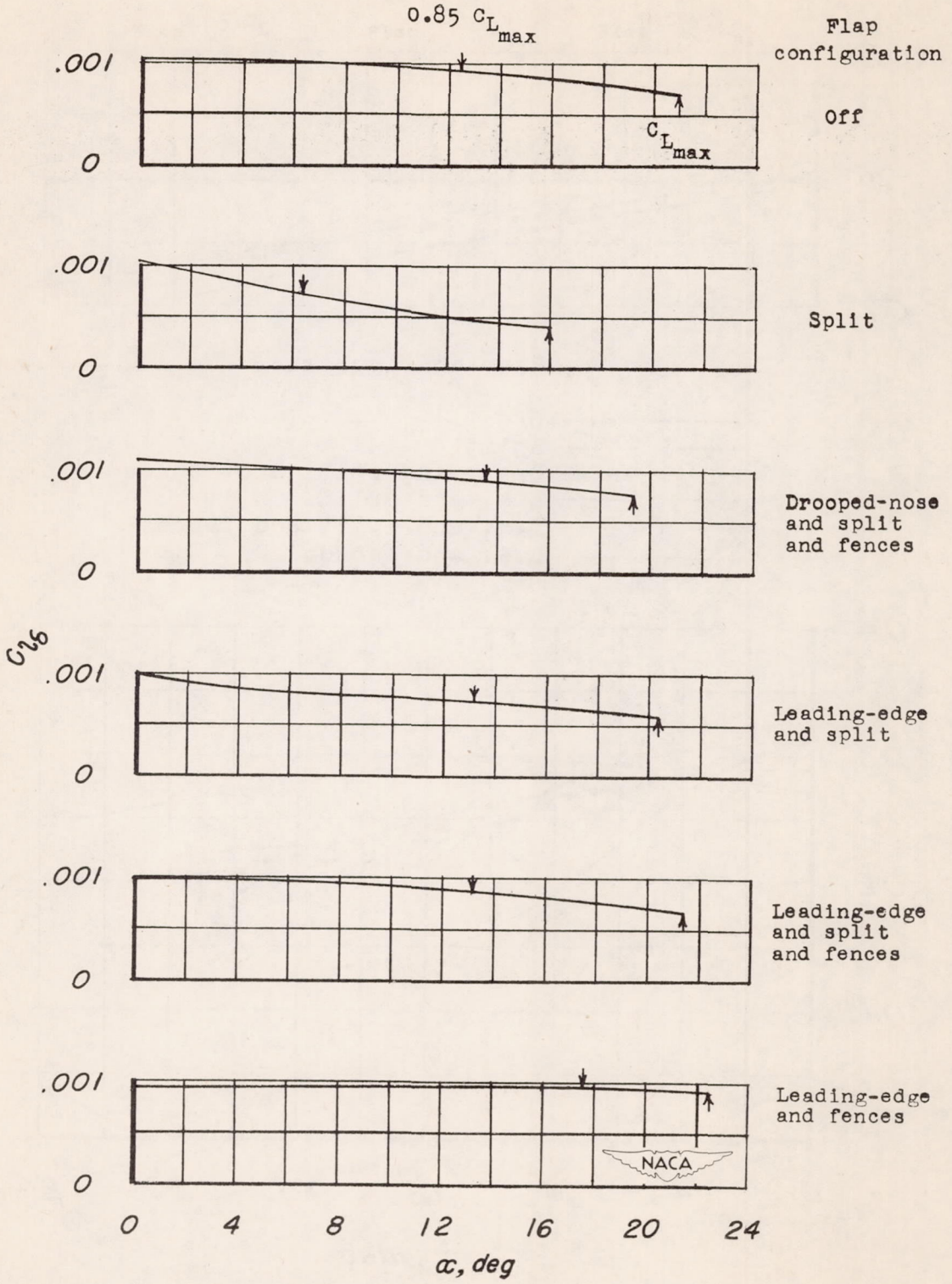

Figure 13.– Effects of high–lift and stall–control devices on aileron effectiveness parameter C_{l_δ}.

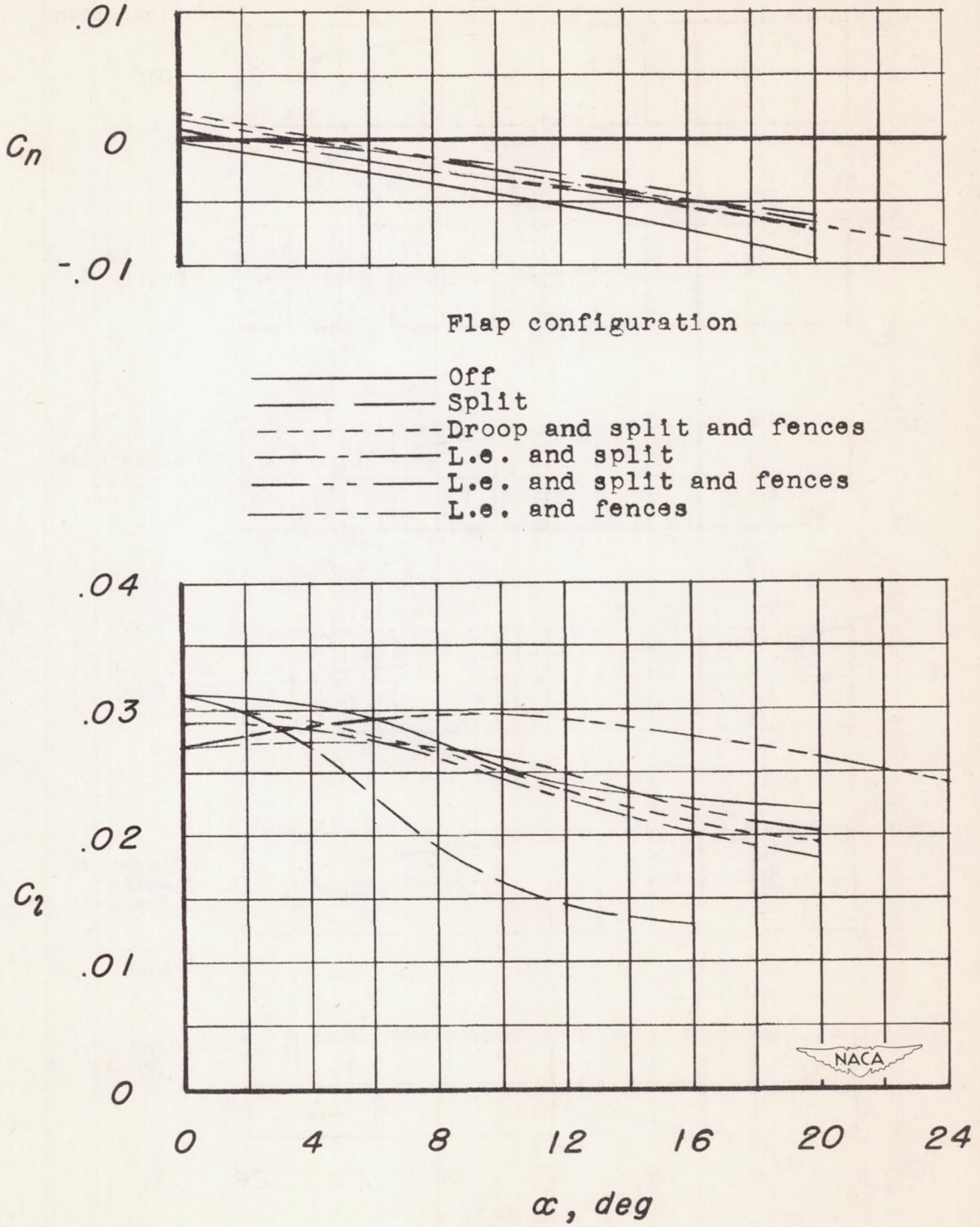

Figure 14.- Rolling- and yawing-moment characteristics for a total aileron deflection of 30°.

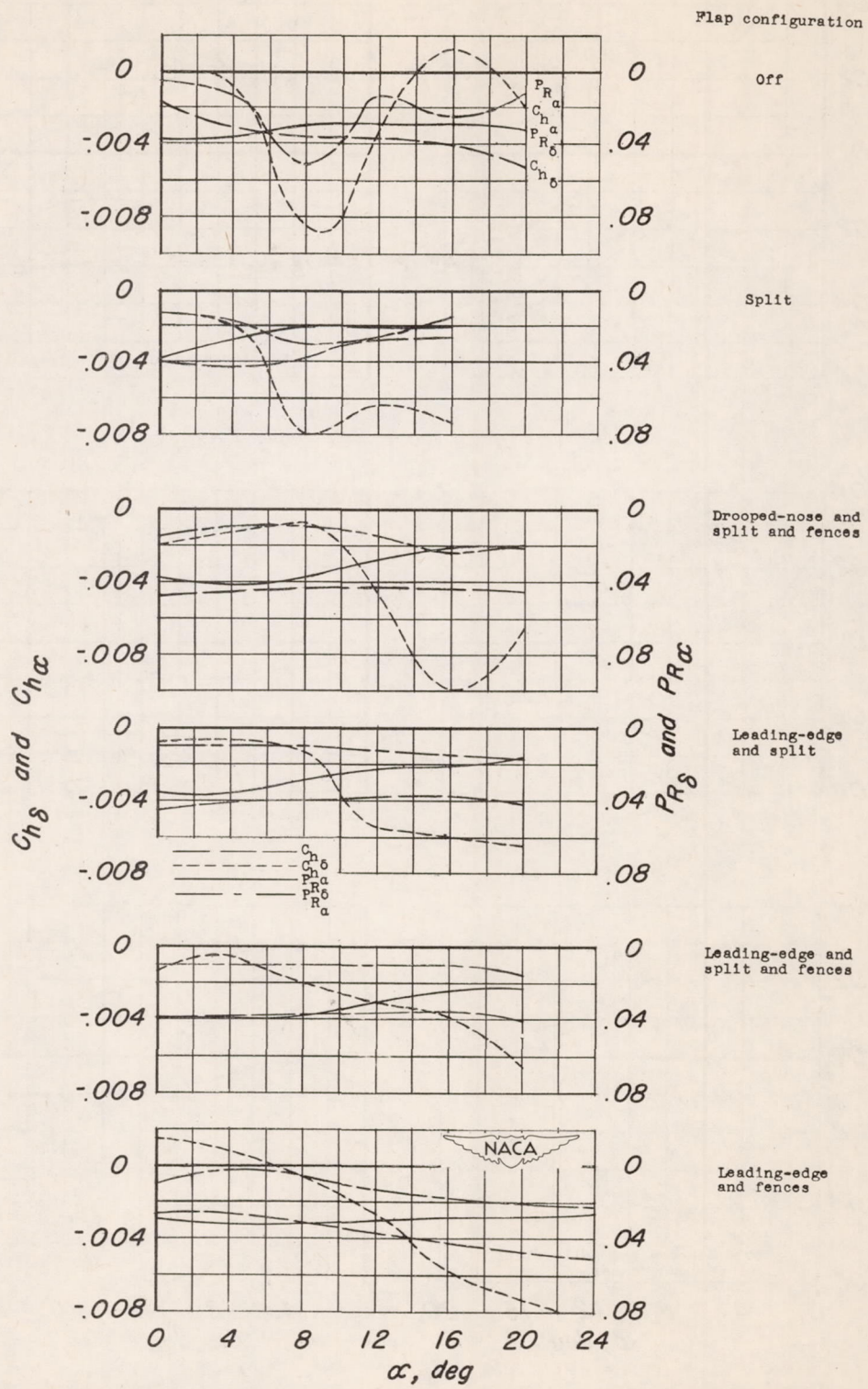

Figure 15.– Effects of high–lift and stall–control devices on the aileron hinge–moment parameters C_{h_δ}, C_{h_α}, P_{R_δ}, and P_{R_α}.

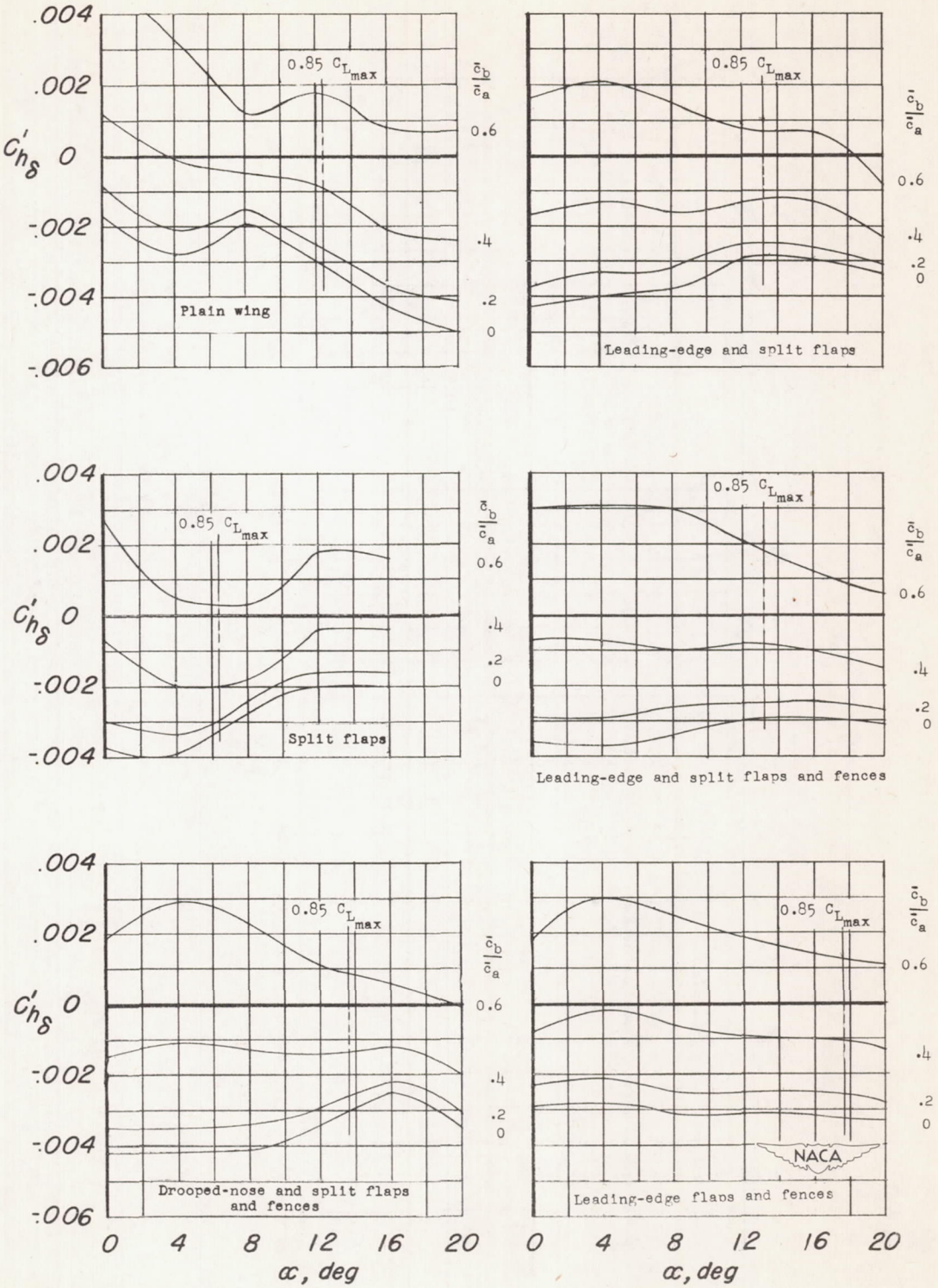

Figure 16.– Effect of various amounts of aerodynamic balance on aileron hinge-moment parameter C'_{h_δ}.

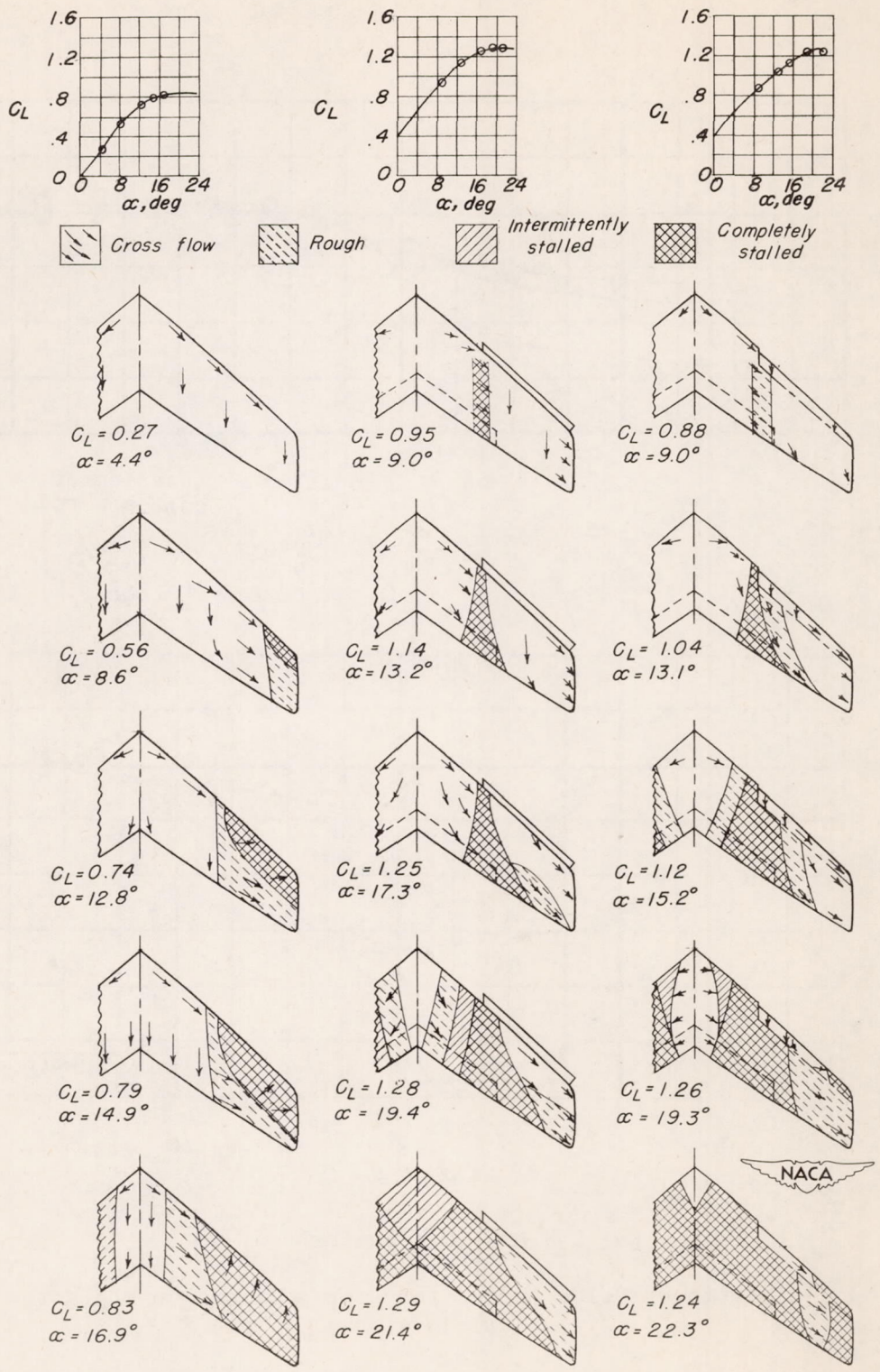

(a) Flaps off. (b) Extensible leading-edge flaps and split flaps. (c) Drooped-nose flaps and split flaps.

Figure 17.- Stalling characteristics of 42° sweptback wing.

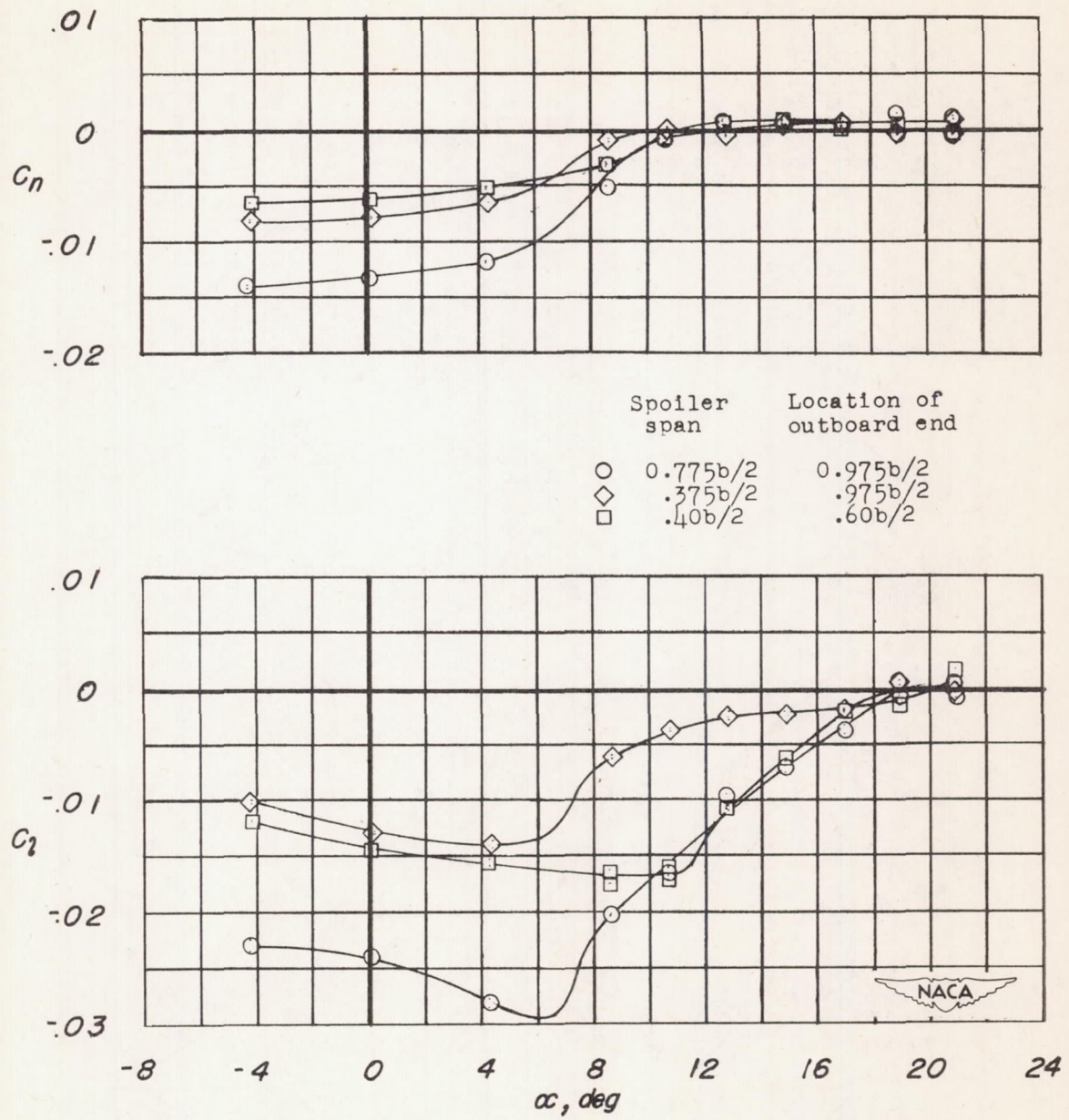

(a) C_l and C_n against α.

Figure 18.– Effects of 0.10c projection step spoilers on characteristics of plain wing.

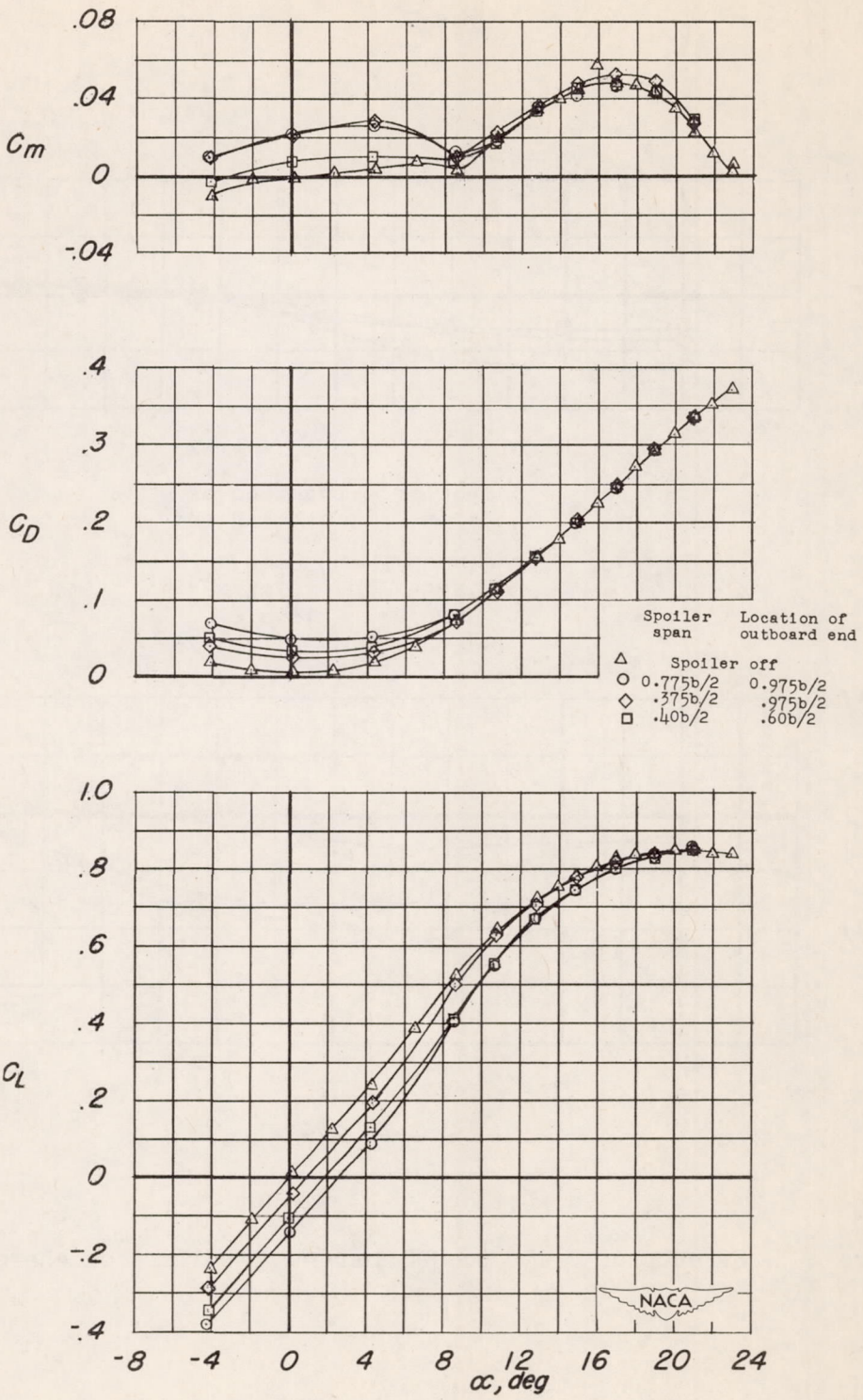

(b) C_L, C_D, and C_m against α.

Figure 18.– Concluded.

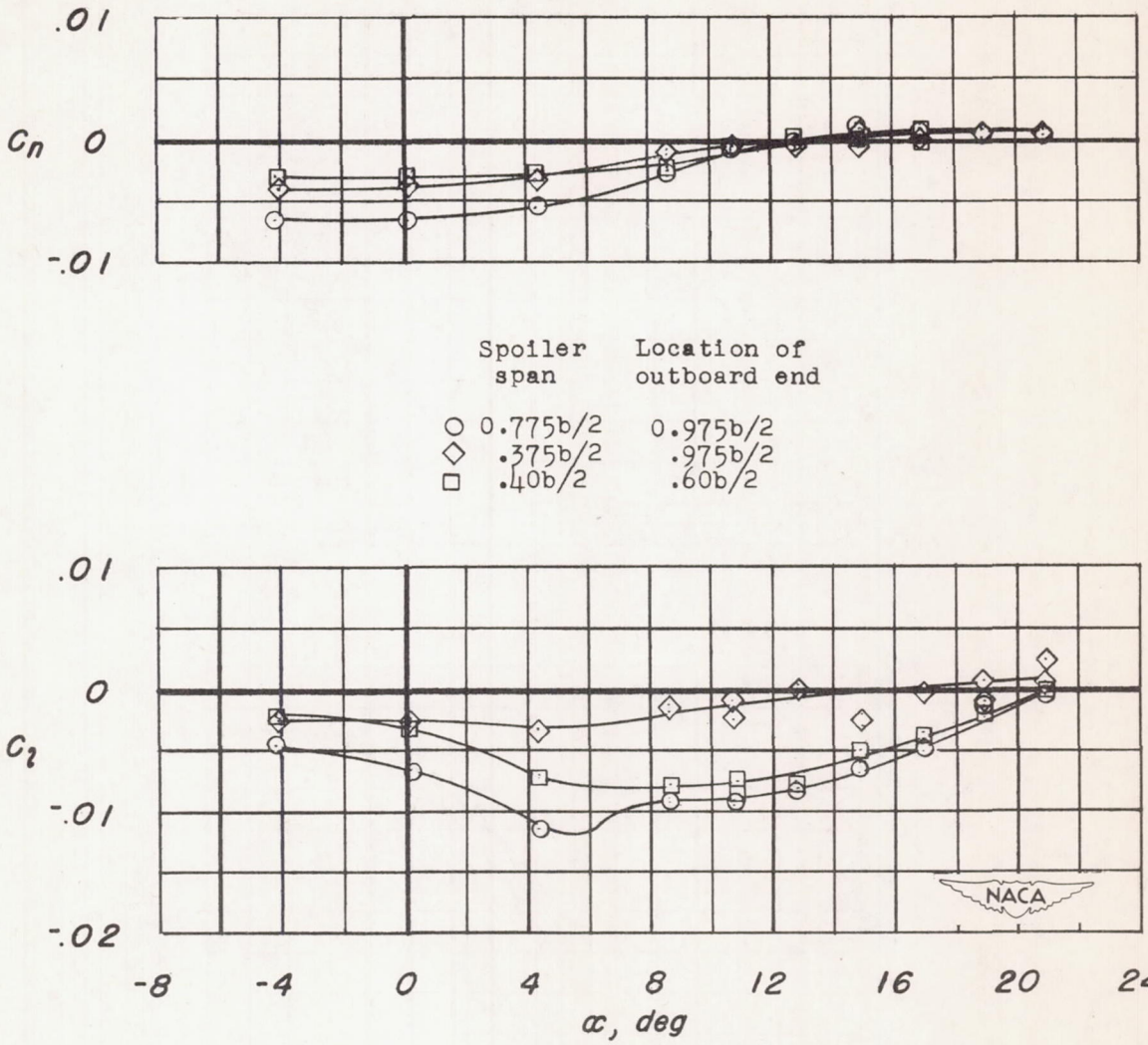

(a) C_l and C_n against α.

Figure 19.– Effects of 0.05c projection step spoilers on characteristics of plain wing.

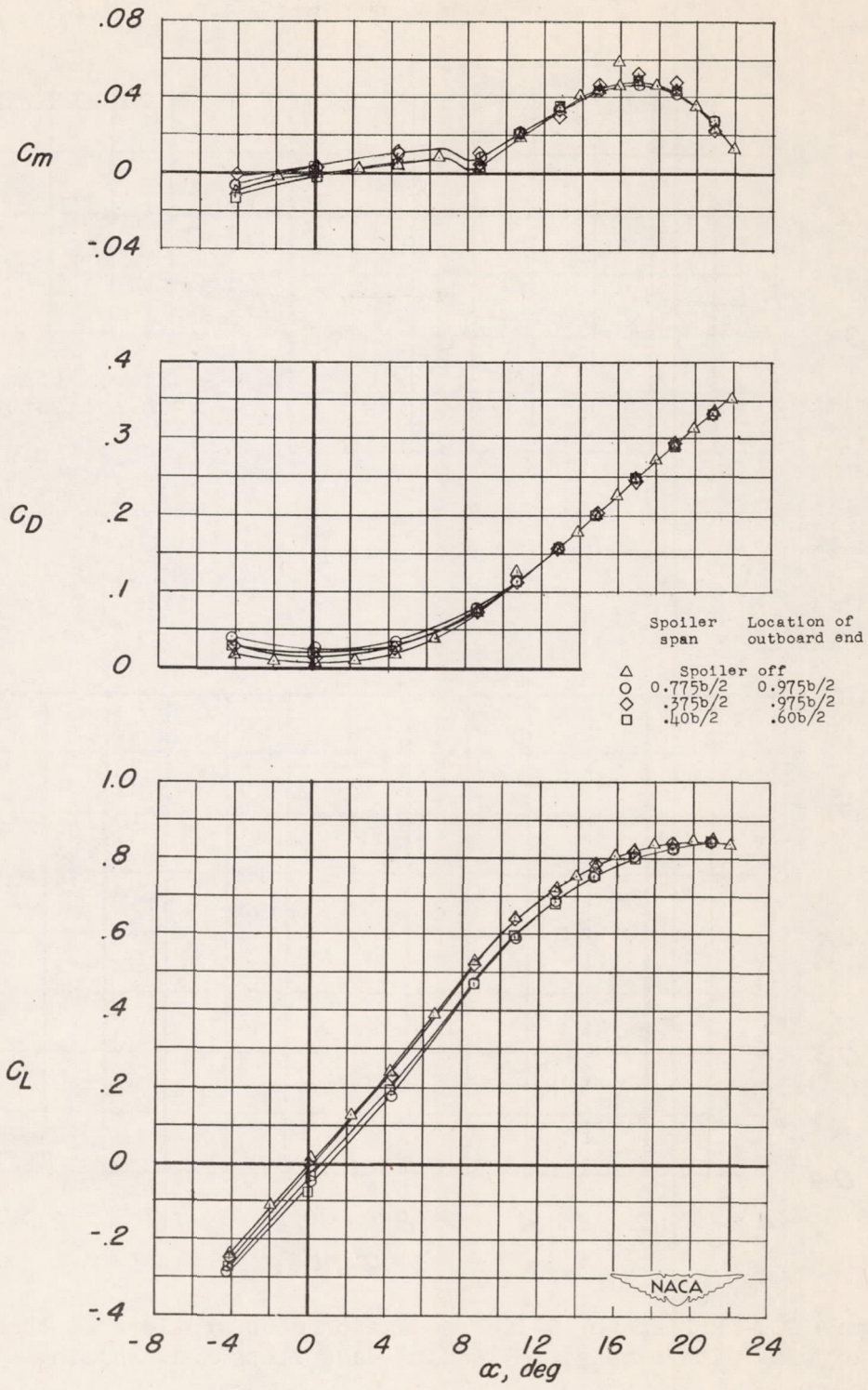

(b) C_L, C_D, and C_m against α.

Figure 19.– Concluded.

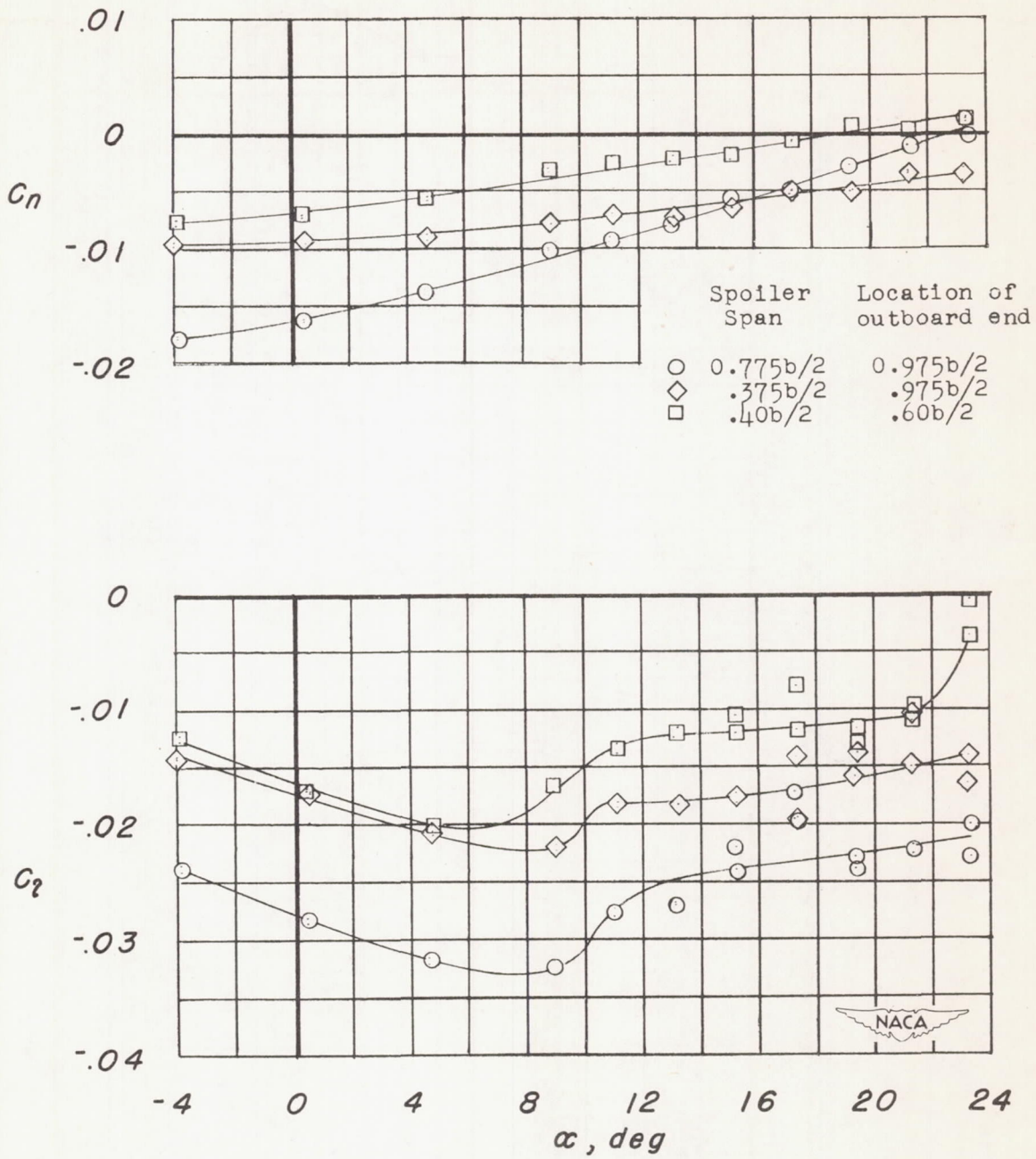

Figure 20.– Effects of 0.10c projection step spoilers on characteristics of wing with extensible leading–edge flaps and trailing–edge split flaps.

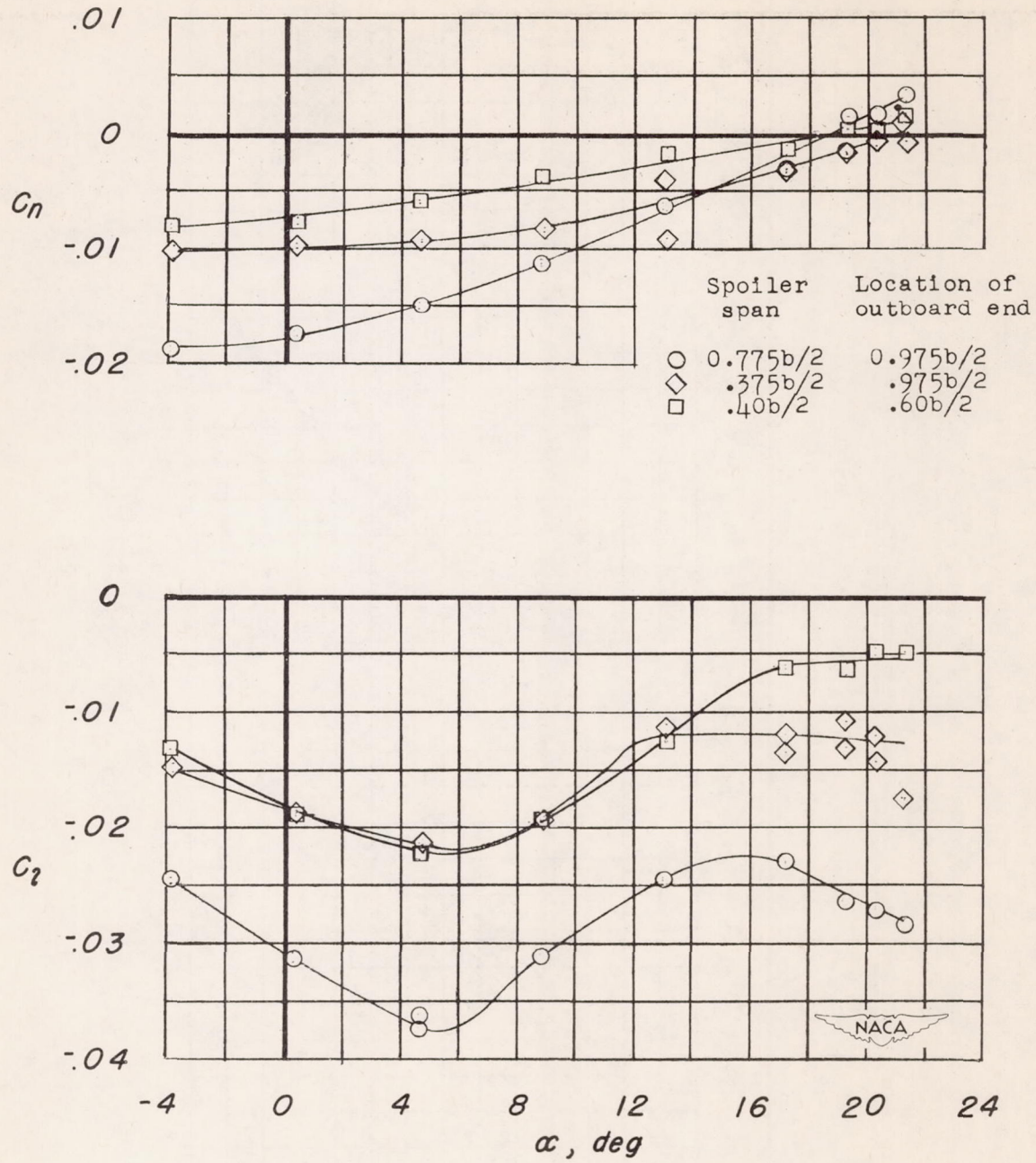

(a) C_l and C_n against α.

Figure 21.– Effects of 0.10c projection step spoilers on characteristics of wing with drooped–nose flaps and trailing–edge split flaps.

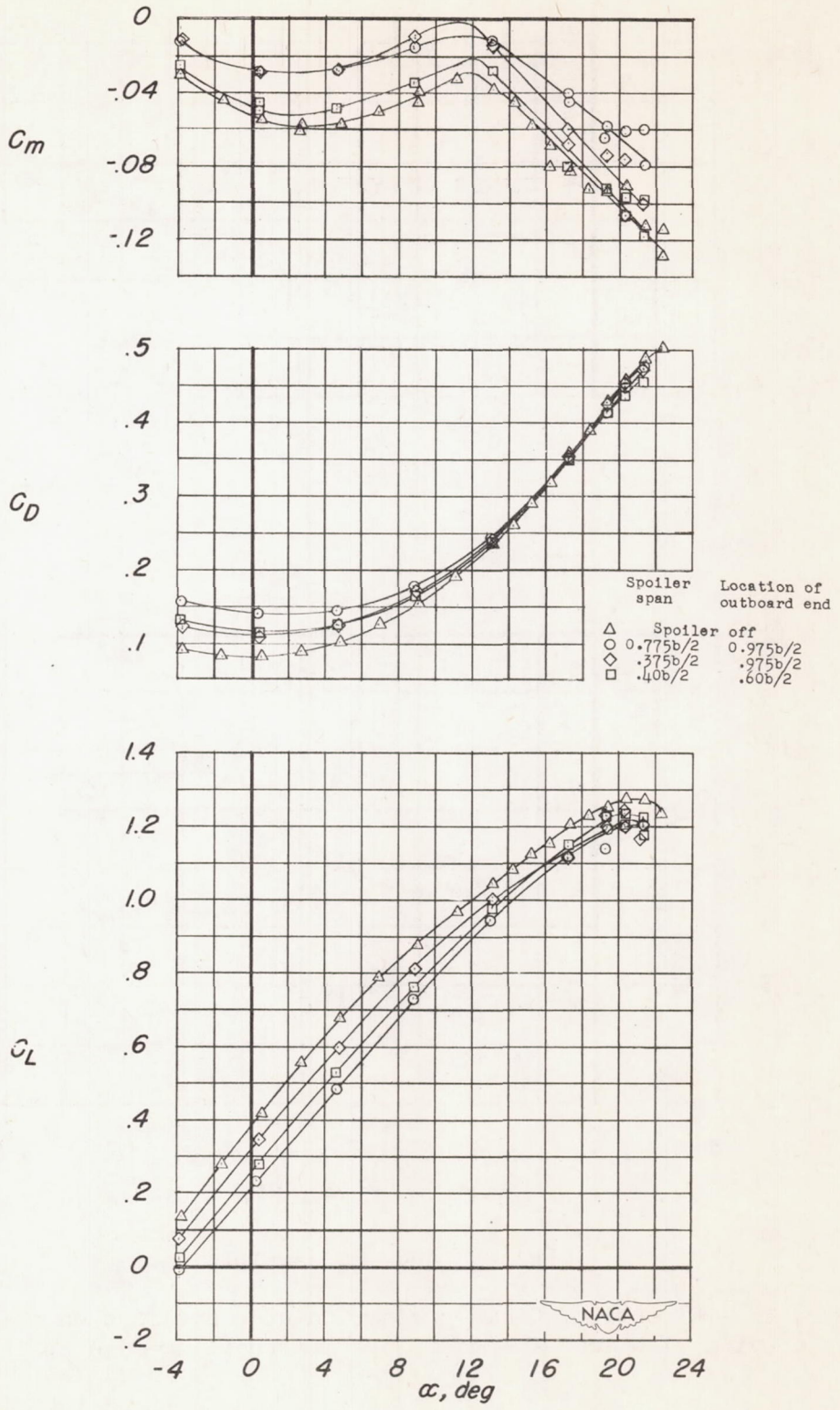

(b) C_L, C_D, and C_m against α.

Figure 21.– Concluded.

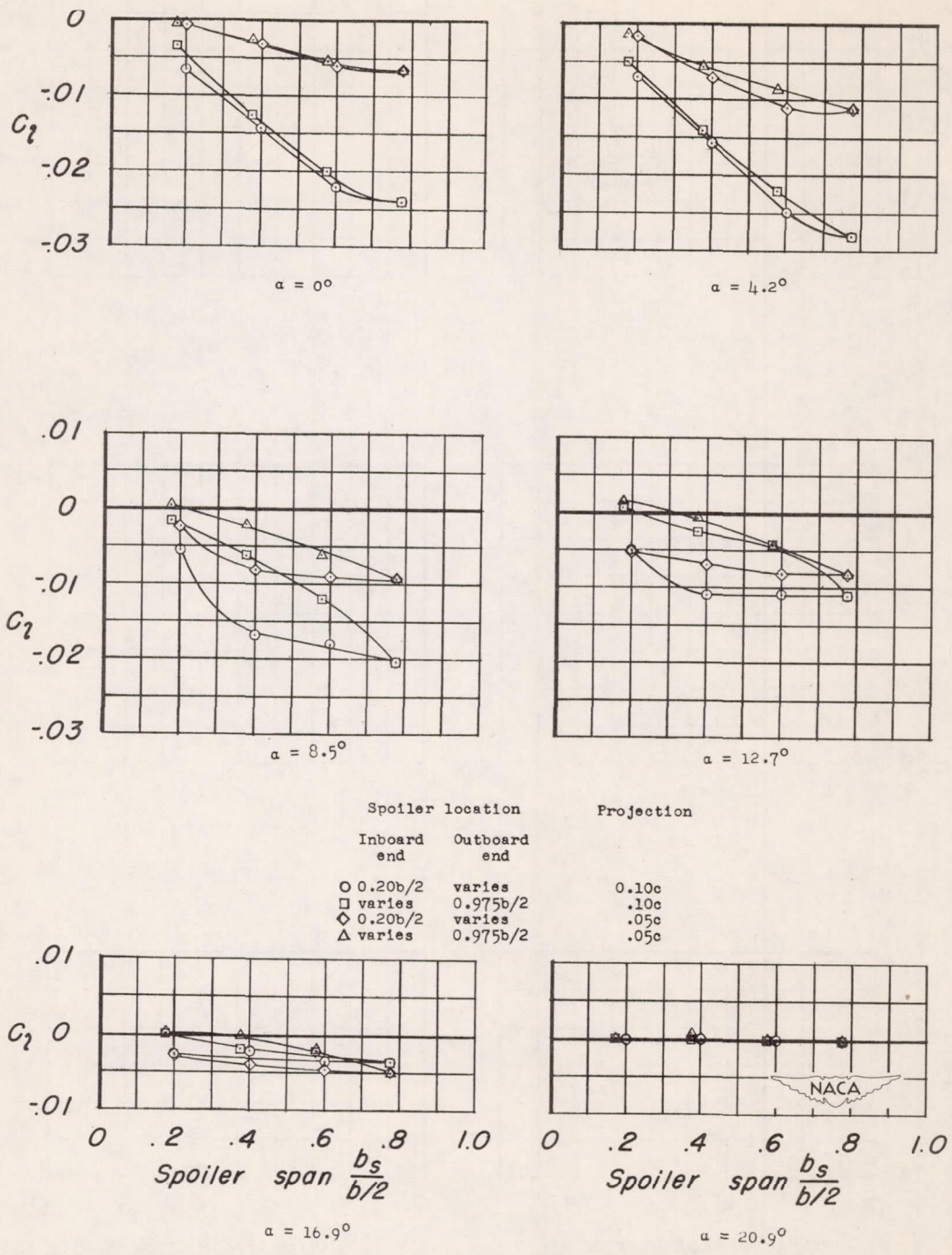

Figure 22.– Variation of rolling-moment coefficient with span of step spoilers on the plain wing. 0.05c and 0.10c spoiler projection.

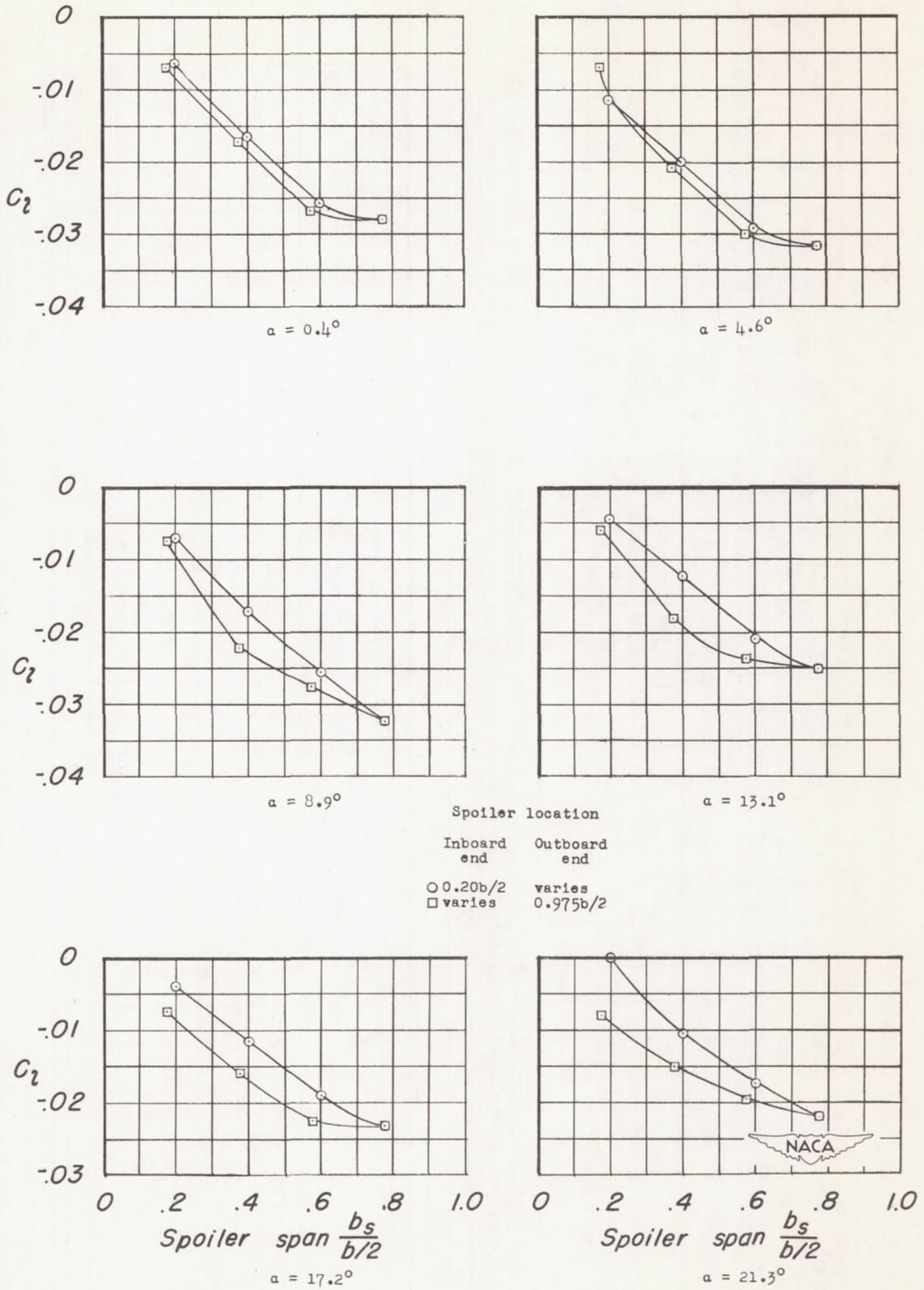

Figure 23.– Variation of rolling–moment coefficient with span of 0.10c projection step spoilers on wing equipped with extensible leading–edge flaps and trailing–edge split flaps.

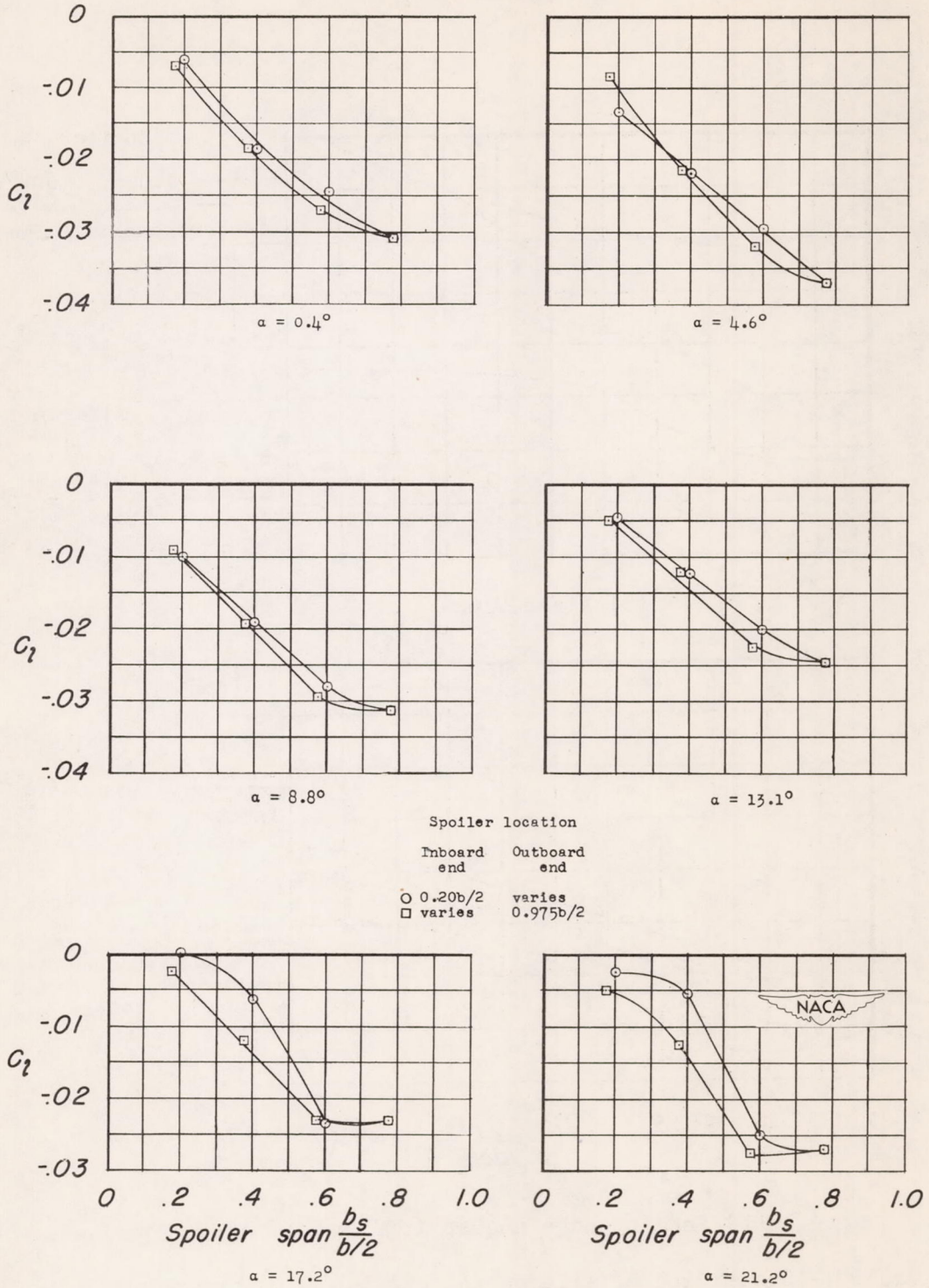

Figure 24.– Variation of rolling-moment coefficient with span of 0.10c projection step spoilers on wing equipped with drooped-nose flaps and trailing-edge split flaps.

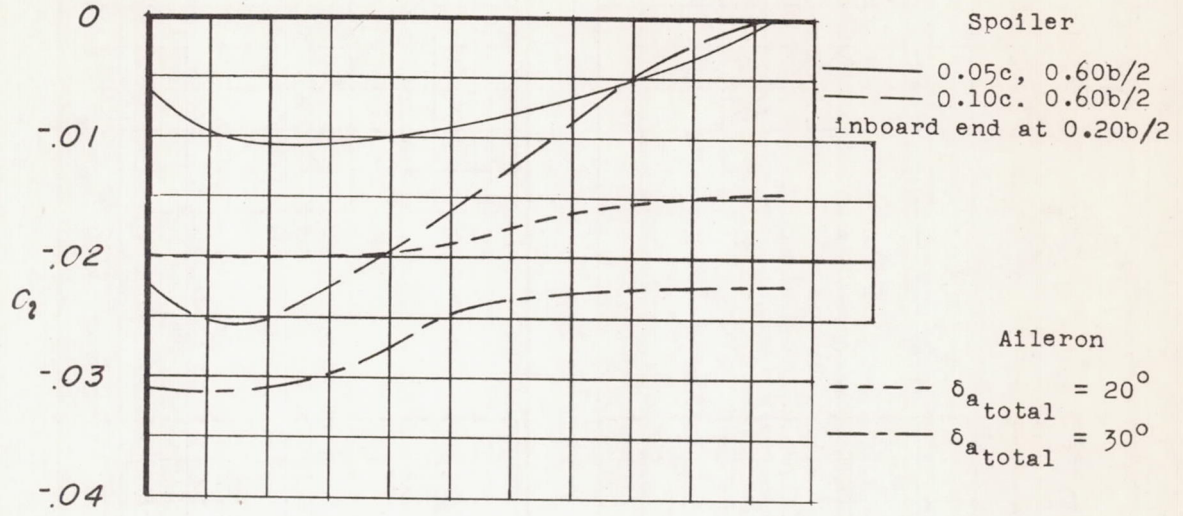

(a) Plain wing.

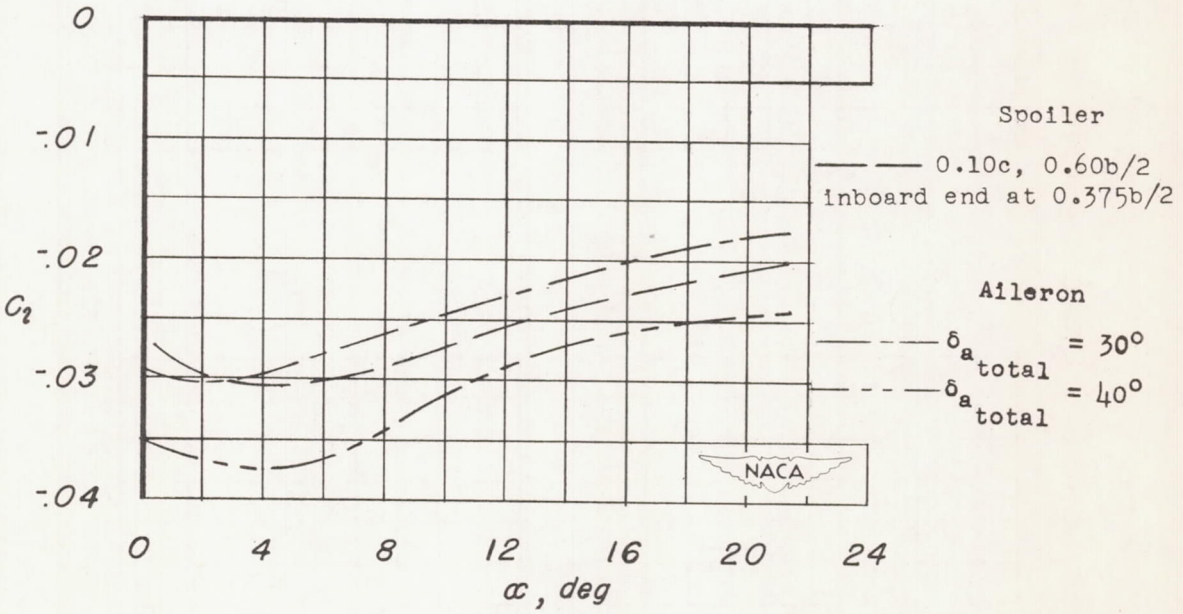

(b) Leading-edge and split flaps.

Figure 25.- Comparison of aileron and spoiler effectiveness.